
# Guide to Leveraging Conducting Polymers and Hydrogels for Direct Current Stimulation

ADVANCED MATERIALS INTERFACES
Open Access
www.advmatinterfaces.de



# Guide to Leveraging Conducting Polymers and Hydrogels for Direct Current Stimulation

*José Leal,* Sebastian Shaner, Lukas Matter, Christian Böhler, and Maria Asplund**

**The tunable electrical properties of conducting polymers (CPs), their biocompatibility, fabrication versatility, and cost-efficiency make them an ideal coating material for stimulation electrodes in biomedical applications. Several biological processes like wound healing, neuronal regrowth, and cancer metastasis, which rely on constant electric fields, demand electrodes capable of delivering direct current stimulation (DCs) for long times without developing toxic electrochemical reactions. Recently, CPs such as poly(3,4-ethylenedioxythiophene) polystyrene sulfonate (PEDOT/PSS) have demonstrated outstanding capability for delivering DCs without damaging cells in culture while not requiring intermediate buffers, contrary to the current research setups relying on noble-metals and buffering bridges. However, clear understanding of how electrode design and CP synthesis influence DCs properties of these materials has not been provided until now. This study demonstrates that various PEDOT-based CP coatings and hydrogels on rough electrodes can deliver DCs without substantial changes to the electrode and the noticeable development of chemical by-products depending on the electrode area and polymer thickness. A comprehensive analysis of the tested coatings is provided according to the desired application and available resources, alongside a proposed explanation for the observed electrochemical behavior. The CPs tested herein can pave the way toward the widespread implementation of DCs as a therapeutic stimulation paradigm.**

## 1. Introduction

Since their discovery in 1977 and subsequent Nobel Prize in 2000, conducting polymers (CPs) have been a breakthrough in material science with a wide range of applications in electronics (e.g., ChemFET, flexible circuits, OLED, mechanical electronics),[1–4] solar cell technology,[5–9] solar water purification,[10] batteries (e.g., supercapacitors),[11–14] and biomedical engineering (e.g., electrode coating for recording and stimulation, drug delivery, scaffolds for tissue engineering).[15–21] The inherent conductivity of these polymers originates from their chemical structure consisting of repeating alternating chains of single and double ($\pi$-$\pi$) carbon bonds, allowing electrons to move freely alongside the polymeric backbone. Furthermore, these materials can be doped through several processes (e.g., chemically, electrochemically, photonically), effectively increasing their electrical conductivity through the buildup of polarons.[22] In addition to their outstanding and tunable electrical performance, CPs are a cost-effective alternative to metals, can be biodegradable and biocompatible, can be synthesized through a wide range of processes, and can be coated on different types of substrates. Amongst the most studied CPs, we find polypyrrole (PPy), polyaniline (PANI), and poly(3,4-ethylenedioxythiophene) polystyrene sulfonate (PEDOT/PSS). All these CPs have been extensively used in biomedical applications for bioelectrical measurements, electrical stimulation, drug delivery, and as bioactuators and biosensors.[23–27] Particularly, the use of PEDOT as a coating for stimulation electrodes has been at the center stage of research in the last decade due to the high electrochemical stability and three-dimensional structure of this polymer,

J. Leal, S. Shaner, L. Matter, C. Böhler, M. Asplund
Department of Microsystems Engineering
University of Freiburg
Georges-Köhler-Allee 201, DE 79110 Freiburg, Germany
E-mail: Jose.leal@blbt.uni-freiburg.de;
maria.asplund@imtek.uni-freiburg.de

The ORCID identification number(s) for the author(s) of this article can be found under https://doi.org/10.1002/admi.202202041.



**DOI: 10.1002/admi.202202041**

J. Leal, S. Shaner, L. Matter, C. Böhler, M. Asplund
Brainlinks-Braintools Center
University of Freiburg
Georges-Köhler-Allee 201, DE 79110 Freiburg, Germany

L. Matter, M. Asplund
Freiburg Institute for Advanced Studies (FRIAS)
University of Freiburg
Albertstraße 19, DE 79104 Freiburg, Germany

M. Asplund
Division of Nursing and Medical Technology
Luleå University of Technology
SE 97187 Luleå, Sweden

M. Asplund
Department of Microtechnology and Nanoscience
Chalmers University of Technology
SE 41296 Gothenburg, Sweden

which allows the charge in the form of ions to be stored within the polymeric matrix to be released later through electrostatic interaction with the electrolyte and the charged polymer chains in a pseudo-capacitive manner.[19,28–30]

Biomedical electrical stimulation with conventional metal electrodes relies on capacitive and pseudo-capacitive reversible faradaic reactions to deliver the required charge to the tissue. All these charge delivery methods are limited by the electrochemical reactions happening at the boundary between electrode and electrolyte, which can develop into unwanted, noxious chemical byproducts that change the environment and damage tissue and electrodes alike (i.e., gas evolution, pH changes, corrosion).[31–33] To avoid damage, biphasic charge-balanced stimulation is used to prevent the onset of such reactions. This stimulation paradigm works with bioelectric signaling pathways that only require a short pulse to elicit the desired response, such as the firing of neurons and muscles but is not compatible with the investigation of biological phenomena which rely on sustained electric fields (i.e., direct currents) relevant when electrical stimulation is to be used as the guiding cue. Several fundamental biological processes, such as cell division, cell differentiation, cell migration, and wound healing, are guided by sustained endogenous electric fields (EFs), which are generated by the tissue and steer cells into action.[34–36] The research of these mechanisms relies on mimicking the bioelectrical cue, wherefore direct current stimulation (DCs) is required. Here, metallic electrodes are not safe, as they polarize with charge delivery during stimulation, increasing their potential above the water-splitting window and developing toxic by-products.[37] To circumvent this limitation, the gold standard for research with DCs in vitro relies on agar bridges, which serve as a buffer between the electrode and the cell media or tissue to be stimulated, effectively hindering the electrochemical by-products from reaching the biological sample during the duration of the experiment.[38] Nonetheless, this solution limits the translation of relevant discoveries into clinical applications where salt bridges cannot be integrated. The ideal electrode material for DCs should be capable of delivering current using only charge injection mechanisms that do not evolve into unwanted electrochemical reactions while still being sufficiently compact to be used within in vitro setups and allow for uncomplicated translation into in vivo clinical applications. Conductive polymers could be the solution to this problem, as they can deliver ionic pseudo-capacitive currents by electrostatic interaction with the electrolyte, given that the polymeric matrix contains mobile ions or can absorb mobile ions from the electrolyte. We have previously demonstrated that PEDOT/PSS electrodes stabilized on sputtered iridium oxide film (SIROF) electrodes can deliver DCs to rat prostate cancer cells MAT-LyLu into a microfluidic device, effectively guiding their direction of movement (i.e., electrotaxis).[16] We hypothesize that all PEDOT-based coatings, in general, are capable of electrolysis-free DCs thanks to their ionic bulk pseudo-capacitance, which can inject or withdraw ions from the electrolyte without undergoing irreversible Faradic charge transfer.

In this work, we investigate a small representative selection of preparations and coating strategies (i.e., electropolymerization, spot-casting, embedding into hydrogel) for PEDOT/PSS. The chosen PEDOT-hydrogel combinations represent two opposite coating methodologies, a precise wafer-scale but costly method versus a less reproducible but cost-effective approach. We have chosen to investigate these versions based on the common denominators PEDOT and styrene sulphonate (SS), with SS included either as a polymeric counter ion (PSS, electropolymerization), as a core-shell complex (PSS solution cast) or with SS as a charged functional group in a polymeric hydrogel backbone (hydrogel-immobilized electropolymerization counter ion). Furthermore, as the substrate has a crucial role in the stability of the polymer,[16,39,40] we explore two different rough substrates (i.e., Sputtered Iridium Oxide Films – SIROF and Laser Induced Graphene – LIG) with additional surface functionalization supporting the longevity of the interface. We demonstrate the stability of different PEDOT-based materials under DCs by measuring the changes in electrode potential over time and using time-lapse imaging and a microfluidic chamber to visualize the electrode's surface and detect gas bubbles that would result from electrolysis.

Additionally, we analyze the stability of the different coatings under cyclic loading through repeated cyclic voltammetry (CV) to determine how repeated charging and discharging of the polymeric matrix influences the electrochemical properties of the electrodes. These experiments are performed on electrodes of different sizes (i.e., active electrode area) and for different thicknesses of the CP coatings. The rationale for investigating multiple thicknesses is to analyze if, by exploiting the three-dimensional volume of the film, it is possible to enhance the DC stimulation performance and compensate for a smaller electrode area by increasing coating thickness. The different PEDOT-based coatings differ in their preparation and coating strategies, which provide a wide range of possibilities depending on the desired application (i.e., microelectrodes, macro electrodes) and available instrumentation.

We demonstrate that all the CPs-versions included in our study are suitable for DCs within the tested timeframe and parameters (10 μA for 2 h) with an initial pseudo-capacitive charge delivery phase (i.e., release of ions) followed by a transition into Faradaic surface processes (i.e., electrolysis) once the ionic content is depleted. The onset of the latter is directly related to the volume of the CP on the substrate electrode. A larger CP volume is expected to increase the duration of the pseudo-capacitive charge delivery phase, as it can contain a higher amount of ions. The volume of the film can either be increased by a larger area or by thicker layers, and our data points to the fact that these two approaches are not interchangeable. A larger electrode area proved to be the most influential parameter in improving the DC stimulation performance of the electrodes. At the same time, an increase in polymeric thickness showed only marginal improvements for the same experiments. Furthermore, a larger area contributed significantly to the stability under cyclic loading of the electrodes, reducing the changes in impedance and charge storage capacity over the testing period.

A straightforward comparison of advantages and disadvantages for each of the tested materials herein was made based on the efficiency and simplicity of fabrication, the obtained charge storage capacity, and the stability of the electrodes under direct current and cyclic loading. Based on these parameters, we show that both electropolymerized PEDOT/PSS on SIROF

and spot-cast PEDOT:PSS on LIG are the most promising candidates for applications in which long-term DCs is required, providing two completely different fabrication technologies and approaches for research. Finally, we propose an explanation of the charge delivery mechanisms happening at the investigated materials during DCs.

## 2. Experimental Section

### 2.1. Electrode Materials

Two different types of polyimide (PI) were used as a base to stabilize the conductive polymers under investigation. PI was processed either as a precursor spin-coated into a thin (5 µm) film and imidized at high temperature (U-Varnish S polyimide, UBE Industries Ltd., Tokyo, Japan) or was processed as a sheet material (A4 – 210 × 297 $mm^2$) which was further laser structured (Kapton 300HN, Dupont, DE USA). On both types of carrier materials, interconnections and electrodes were patterned with active areas ranging from 1 to 20 $mm^2$. The cleanroom-processed thin-film devices allowed for higher precision and smaller feature size. Here, two additional designs of 0.5 $mm^2$ and 20 $mm^2$ separated into five smaller 4 $mm^2$ areas were fabricated (**Figure 1**A). Sputtered iridium oxide film (SIROF) electrodes were patterned according to previously published protocols for thin-film PI.[39,40] In brief, we used reactive sputtering of iridium (Ir) in an oxygen ($O_2$) rich atmosphere to deposit SIROF on a base layer of sputtered platinum (Pt). The exposed metallization was encapsulated by an additional 5 µm thick PI layer. The active electrode and interconnection sites were opened through reactive ion etching (RIE) in an $O_2$ atmosphere, by which the electrode area was precisely defined. Afterward, electrodes were ready for functionalization. They were coated with adhesion promoters at the wafer level (when applicable), released from the wafer, and electrically contacted through soldering and subsequent insulation of the solder joint with nylon-based adhesive.

The Laser-Induced Graphene (LIG) electrodes were fabricated through laser carbonization of 75 µm thick Kapton sheets with a carbon dioxide ($CO_2$) laser engraver (Versa Laser 2.30, ULS Inc., AZ USA) with a wavelength of 10.6 µm. After the rastering process, which carbonized the Kapton to form active electrode sites, tracks, and interconnects (4.8 W, 15.2 mm $s^{-1}$, 1000 PPI); the devices were cut (12 W, 25.4 mm $s^{-1}$), and a nylon-based insulation layer was manually added onto the tracks. The different electrode substrates were subsequently coated with poly(3,4-ethylenedioxythiophene) polystyrene sulfonate PEDOT PSS-based conductive polymers through several alternative coating methods to identify which process resulted in the most favorable material characteristics. Both electrode substrates were coated with electropolymerized PEDOT/PSS (ePEDOT) and spot-cast pure PEDOT:PSS hydrogel (hPEDOT). Additionally, the SIROF electrodes were functionalized with the synthetic hydrogel P(DMAA-co-5%MABP-co-2.5%SSNa) (PDMAAp) consisting of dimethylacrylamide (DMAA) (92.5 mol%), the photo crosslinker 4-methacryloyloxy benzophenone (MABP) (5 mol%) and sodium 4-styrenesulfonate (SSNa) (2.5 mol%)[29,41] into which interpenetrating PEDOT/PSS chains were electrochemically polymerized (Figure 1B). Furthermore, control samples were prepared featuring only the electrode substrate (i.e., SIROF or LIG), and when applicable, specific surface functionalization protocols without added PEDOT were also analyzed. Further details on the fabrication steps can be found in the supplemental data (S1).

### 2.2. Electrochemical Characterization

Regardless of coating technology, all electrodes were electrochemically characterized before and after all experiments. For this, an Autolab potentiostat/galvanostat (PGSTAT 204,

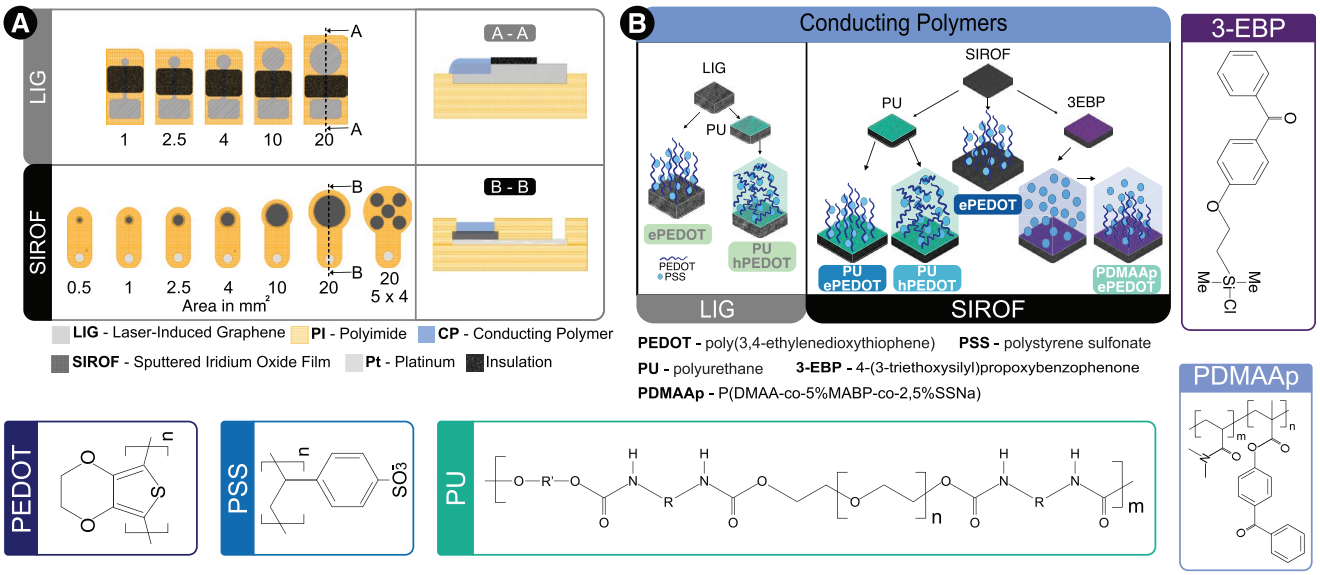


**Figure 1.** A) Electrode designs and cross-section for LIG and SIROF devices of increasing active area. B) Possible conducting polymer coatings for each substrate material with intermediate surface functionalization. Chemical structure for the polymers used during these steps.

Metrohm Autolab B.V., Filderstadt, Germany) in a three-electrode configuration was used, with a stainless-steel sheet (≈2 $cm^2$) as the counter electrode (CE), a silver/silver-chloride (Ag/AgCl, BASI, USA) as reference electrode (RE) and the material under investigation as working electrode (WE). Electrochemical characterization was performed in 15 ml of 0.01 M phosphate-buffered saline (PBS, Sigma Aldrich, USA) according to guidelines proposed for the characterization of electrodes for bioelectronic applications and was the same for all devices unless otherwise stated: [42]

1. Measurement of Open Circuit Potential (OCP) versus Ag/AgCl
2. Cyclic Voltammetry (CV) → 5 cycles between –0.6 V and +0.9 V at 0.1 V $s^{-1}$ (starting and ending at OCP)
3. Electrochemical impedance spectroscopy (EIS); → single sine excitation with 10 mV amplitude, 5 points/decade between $f$ = 0.1 Hz – 100 kHz; **50 mV amplitude for cyclic stressing

### 2.3. Electrochemically Polymerized PEDOT/PSS (ePEDOT)

For the coating of any electrode with electrochemically polymerized PEDOT/PSS (ePEDOT), an aqueous solution containing sodium polystyrene sulfonate (NaPSS, 5 mg $ml^{-1}$) and 3,4-ethylenedioxythiophene monomers (EDOT, 0.01 M) (Sigma Aldrich, MO, USA), in combination with a high precision potentiostat/galvanostat (PGSTAT 204) were used. The polymerization was potentiostatically driven at 0.9 V in a three-electrode setup in which the probe to be coated served as the working electrode (WE), a silver/silver-chloride (Ag/AgCl, BASI, USA) electrode as the reference (RE), and a stainless-steel sheet (≈2 $cm^2$) as the counter electrode CE. The charge delivered was monitored, and the charge density was used as a reference point to control the polymer thickness, which increases at a rate of ≈7 nm (mC $cm^{-2}$)$^{-1}$.[16] Detailed information about the preparation steps can be found in Material S2, Supporting Information.

### 2.4. Spot-Cast PEDOT:PSS Hydrogel (hPEDOT)

The coating with PEDOT:PSS hydrogel (hPEDOT) required an initial surface functionalization step with polyurethane (PU) of the electrodes, which was applied to both SIROF and LIG unless otherwise stated. The process started with surface treatment of the electrodes in air plasma at 100 W for 5 min to functionalize them with hydroxyl (–OH) groups (Femto, Diener Electronic, Ebhausen, Germany), followed by their immersion in a (3-Aminopropyl)trimethoxysilane (APTMS, 1% v/v) solution (Sigma Aldrich, MO, USA), which adds amine ($–NH_2$) groups to the electrode's surface. After 60 min in APTMS, the electrodes were cleaned with DI water, dried, and subsequently coated with hydrophilic polyurethane (PU, 1% w/v) (AdvanSource HydroMed D3, USA) dissolved in ethanol (95% EtOH) using a dip-coater (ND-R Rotary Dip Coater, Nadetech Innovations, Spain). The PU-coated electrodes were placed on a hot plate at 80 °C for 60 min to evaporate the remaining solvent, which resulted in a stable hydrophilic polymer adhesive layer, which PEDOT:PSS can interpenetrate according to procedures published by Inoue et al.[43] The PU-functionalized electrodes were either coated with ePEDOT following the previously described protocol or alternatively, a pure PEDOT:PSS hydrogel precursor was spot-cast on the substrate following the protocol by Lu et al.[44] In this case, a PEDOT:PSS solution (Sigma Aldrich, 1.3% w/v) was mixed with dimethyl sulfoxide (DMSO) and deionized water to form a dispersion of 15% v/v DMSO with the remaining percentage being deionized water.[44–46] This dispersion was manually cast onto the electrode while keeping the substrate at a stable temperature (60 °C) on a hot plate. The thickness of the hPEDOT layer added was controlled indirectly by keeping the volume of PEDOT:PSS-DMSO dispersed at 1 µl $mm^{-2}$, thus normed to the electrode's area. By repeating the spot-casting procedure (typically at 5 min intervals), it was possible to form thicker layers of the hydrogel. After spot-casting, the electrodes were annealed at 60 °C for 12 h to evaporate water and allow interpenetration of the PEDOT:PSS into the PU adhesion promoter, followed by a second annealing step at 130 °C for 2 h in which the DMSO was evaporated, and strong inter-PEDOT bridging could take place.[47] Detailed information about the preparation steps can be found in Material S2, Supporting Information.

### 2.5. Interpenetrating PEDOT/PSS in PDMAAp Hydrogel (PDMAAp-ePEDOT)

The functionalization of electrodes with the synthetic hydrogel P(DMAA-co-5%MABP-co-2,5%SSNa) (PDMAAp) was performed according to the protocols described by Kleber et al.[29,48] starting by spin-coating of the electrodes with 1.5 ml of the ultraviolet (UV) light reactive 4-(3-triethoxysilyl)propoxybenzophenone (3-EBP) silane, followed by the annealing on a hot plate at 120 °C for 30 min and cleaning of residual silane with toluene. This functionalization provided a covalently attached anchor on the SIROF layer for the PDMAAp hydrogel.[49] Afterward, the entire wafer was dip-coated in the PDMAAp hydrogel solution (90% EtOH, 30 mg $ml^{-1}$ PDMAAp), forming a thin layer (≈1 µm) of hydrogel precursor. The electrode sites were illuminated through a foil mask with a total dose of 2 J $cm^{-2}$ using a mask aligner (MA6/BA6, Carl Zeiss AG, Jena, Germany) with an I-Line filter (365 nm), which cross-linked the 3-EBP silane with the methacryloyloxy benzophenone (MABP) within the hydrogel. These steps (dip-coating + UV cross-linking) can be repeated if necessary to increase the thickness of the PDMAAp hydrogel by approximately 1 µm layer$^{-1}$.[29,48] After removing the excess PDMAAp in a 90% ethanol solution, the electrodes were released from the wafer, soldered, and insulated before electropolymerization of PEDOT/PSS. The electrodes were soaked for 1 hour in an aqueous solution of DI water with 0.01 M EDOT without any supporting electrolyte since the hydrogel backbone already contains 2.5% sodium 4-styrene sulfonate (NaSS), which serves as counterion during polymerization. Electropolymerization of PEDOT/PSS into the hydrogel was driven galvanostatically at a current density of $j$ = 300 µA $cm^{-2}$ using the charge passing through as a proxy to control the amount of PEDOT formed in the hydrogel. Afterward, the electrodes

were immersed in DI water for 12 h to extract unreacted monomers from the hydrogel matrix. Detailed information about the preparation steps can be found in Material S2, Supporting Information.

### 2.6. Stability Under Direct Current Stimulation

Direct current stimulation (DCs) capability was analyzed for all carriers and coating materials described here for electrodes of different sizes and polymer thicknesses. A constant current of 10 µA was applied over 2 h, equivalent to 72 mC of charge, within a tailor-made electrochemical cell. This current corresponds to a current density of $j$ = 2000 – 1000 – 400 – 250 – 100 – 50 µA cm$^{-2}$ for the electrodes of $A$ = 0.5 – 1 – 2.5 – 4 – 10 – 20 mm$^2$, respectively. The expected potential excursions over the stimulation period within the pseudo-capacitive and the faradaic charge delivery phases are depicted alongside the applied current in **Figure 2**A (insert). The cell consisted of a laser-cut polymethyl methacrylate (PMMA) reservoir sandwiched between two glass slides. The glass was attached to the reservoir using laser-cut PMMA-based double-sided pressure-sensitive adhesive (dsPSA, Adhesives Research, 90445Q film, Glen Rock, PA, USA) (Figure 2A). The front-side adhesive featured a microchannel of 5 mm length ($L$), 80 µm height ($h$), and 450 µm width ($w$) filled with PBS, thus forming a geometrically well-defined liquid pathway interconnecting the reservoirs containing the two stimulation electrodes. This design allowed the electric field (EF) and electrical resistance inside the channel to be precisely controlled.

Furthermore, the cell provided optical access to the electrodes during stimulation. All materials were cut with a $CO_2$ laser engraver (Versa Laser 2.30, ULS Inc., AZ USA). The reservoirs and channels were filled with 0.01 M PBS, and the electrodes were entirely submerged in the solution. The WE and CE were chosen to be of identical materials and sizes for these measurements. They were connected to an Autolab potentiostat/galvanostat in a two-electrode configuration in which the CE and RE were shorted. The OCP between the WE (anode) and CE/RE (cathode) was measured for 2 min until it stabilized at a value lower than 10 mV, verifying that both electrodes were in electrochemical equilibrium. Subsequently, the current was driven through the circuit using the galvanostatic mode of the potentiostat where the potential changes of the stimulation cell were recorded. It should be noted that this potential represents the contribution of both the WE and CE as well as the ohmic drop at the micro channel ($V_{channel}$ = 1.13 V for PBS at 25 °C $\sigma_{PBS}$ = 1.23 mS mm$^{-1}$). A digital microscope (Dino-lite, AnMo Electronics Corporation, Taiwan) was used to monitor tentative changes at the electrodes' surface during stimulation. Time-lapse images were captured at intervals of 2 min during the entire stimulation. Once the stimulation concluded, the electrodes were placed in a 15 mL beaker with fresh PBS. Both WE and CE were electrochemically characterized by CV and EIS measurements to measure changes in electroactivity. Additionally scanning electron microscopy (SEM) images of stimulated electrodes were taken with a Helios 5 DualBeam FIB-SEM (Thermo Fisher Scientific, MA, USA) after sputtering 7 nm gold on them with a CCU-010 sputter machine (Safematic, Zizers, CH). The sample types analyzed are outlined in **Table 1**.

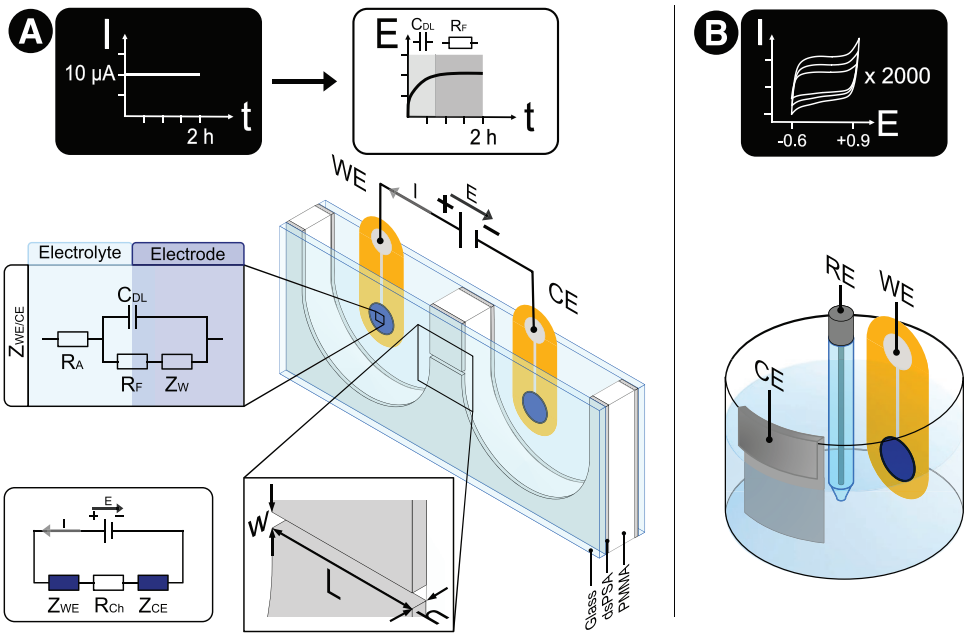


**Figure 2.** Schematic representation of setup used for electrode characterization. A) two-electrode direct current (DC) stimulation in an observation chamber with a microfluidic channel ($w$: 450 µm, $h$: 80 µm, $L$: 5 mm). Expected electrode potential changes with an initial capacitive/pseudo-capacitive region, followed by the onset of faradaic reactions. Equivalent circuit for electrochemical cell consisting of the microfluidic channel resistance $R_{Ch}$ in series with the Working ($Z_{WE}$) and Counter ($Z_{CE}$) electrode impedances. Equivalent circuit of electrode impedance with access resistance ($R_A$), Faradaic resistance ($R_F$), Warburg impedance ($Z_w$), and double layer capacitor ($C_{DL}$). B) Cyclic stressing using CV in a three-electrode setup with stainless-steel counter electrode **CE**, silver/silver chloride reference electrode **RE,** and device under investigation as working electrode **WE**.

**Table 1.** Electrode type and sizes and conductive polymer type and thickness for DC stimulation and cyclic loading (*all PDMAAp electrodes were coated with ≈1 µm hydrogel before PEDOT electropolymerization).

| SIROF electrodes | | | LIG electrodes | | |
|---|---|---|---|---|---|
| Varying area, same polymer thickness | | | | | |
| Area | [mm$^2$] | 0.5 – 1 – 2.5 – 10 – 20 – (5 × 4) | Area | [mm$^2$] | 1 – 2.5 – 10 – 20 |
| **Coating** | **Proxy for thickness** | **Value** | **Coating** | **Proxy for thickness** | **Value** |
| ePEDOT | [mC cm$^{-2}$] | 300 | PU-hPEDOT | [µl mm$^{-2}$] | 1 |
| PU-ePEDOT | | | | | |
| PU-hPEDOT | [µl mm$^{-2}$] | 1 | | | |
| PDMAAp-ePEDOT | [mC cm$^{-2}$] | 300 | | | |
| Same area, varying polymer thickness | | | | | |
| Area | [mm$^2$] | 4 | Area | [mm$^2$] | 4 |
| **Coating** | **Proxy for thickness** | **Value** | **Coating** | **Proxy for thickness** | **Value** |
| ePEDOT | [mC cm$^{-2}$] | 100 – 300 – 500 | ePEDOT | [mC cm$^{-2}$] | 100 – 300 – 500 |
| PU-ePEDOT | | | | | |
| PU-hPEDOT | [µl mm$^{-2}$] | 1 – 2 – 3 | PU-hPEDOT | [µl mm$^{-2}$] | 1 – 2 – 3 |
| PDMAAp*-ePEDOT | [mC cm$^{-2}$] | *(~1 µm PDMAAp) 100 – 300 – 500 | | | |

### 2.7. Stability Under Cyclic Load

The electrochemical stability of the different electrodes and coatings, as well as their interface, was evaluated using an electrochemical stress test, repeatedly driving the electrodes through their oxidized and reduced states (i.e., cyclic voltammetry).[42] The electrodes were subjected to 2000 cycles of ramping potentials between –0.6 V and +0.9 V at 0.1 V s$^{-1}$ in a three-electrode configuration (Figure 2). The test was performed at room temperature, and the setup was contained inside a closed container to prevent evaporation. Initially, 5 CV cycles were recorded, followed by one EIS sweep as described in Section 2.5 to determine the baseline of the electrode. The electrodes underwent 199 CV cycles without storing the current or potential values, followed by one CV cycle and EIS measurement in which the values were stored. This procedure was repeated every 200 cycles until 2000 cycles were reached. The CSC of the recorded CVs and the magnitude of the impedance at a frequency of 1 Hz were used to analyze and compare the effect of cyclic loading on the different coatings and electrode sizes. Low frequencies were chosen, as in this frequency range, the electrode area is more determining of the total impedance due to the contribution of the double layer capacitance $C_{DL}$ and the capacitive behavior of CP coatings.[50] An overview of the sample categories investigated through CV stressing is listed in Table 1.

### 2.8. Sample Preparation

Three identical electrodes were prepared for each material category and parameter to investigate the interaction between the electrode's size, coating thickness, and coating strategy, as well as the impact of these parameters on the electrochemical characteristics. Two were used to test stability during DC stimulation (Section 2.6), and one was used to test stability under cyclic loading (Section 2.7). Our study includes two parametric investigations. First, we investigated the influence of electrode size in combination with different electrode materials and coatings, analyzing both performance under DCs and cyclic load. Second, we investigated the impact of the thickness/volume of the coating on the DCs characteristics. For the latter, all electrodes had the same active surface of 4 mm$^2$, and three different thicknesses of the CPs were prepared and analyzed, as listed in Table 1. Electrodes coated with PDMAAp were the only exception, as the hydrogel coating remained the same for all electrodes at ≈1 µm thickness, and the amount of PEDOT inside varied.

## 3. Results

### 3.1. Electrode Preparation

Conducting polymers have hybrid charge transfer properties and interact with the electrolyte electrostatically and ionically. Thus, as their volume allows them to store and mobilize charged ions, an increase in the CP volume increases the charge storage capacity. Consequently, by increasing the polymer thickness, smaller electrodes may achieve similar electrochemical properties as larger electrodes with a thinner coating.[51] As expected, larger electrode areas deliver higher currents and exhibit lower impedances for the CV and EIS plots, respectively (**Figure 3**A). Furthermore, the increment of available volume for charge storage through increased CP thickness is noticeable upon investigating the electrode's electrochemical properties from both CV and EIS (Figure 3C). Even the thinnest applied CP layers demonstrated an increase in current delivery and

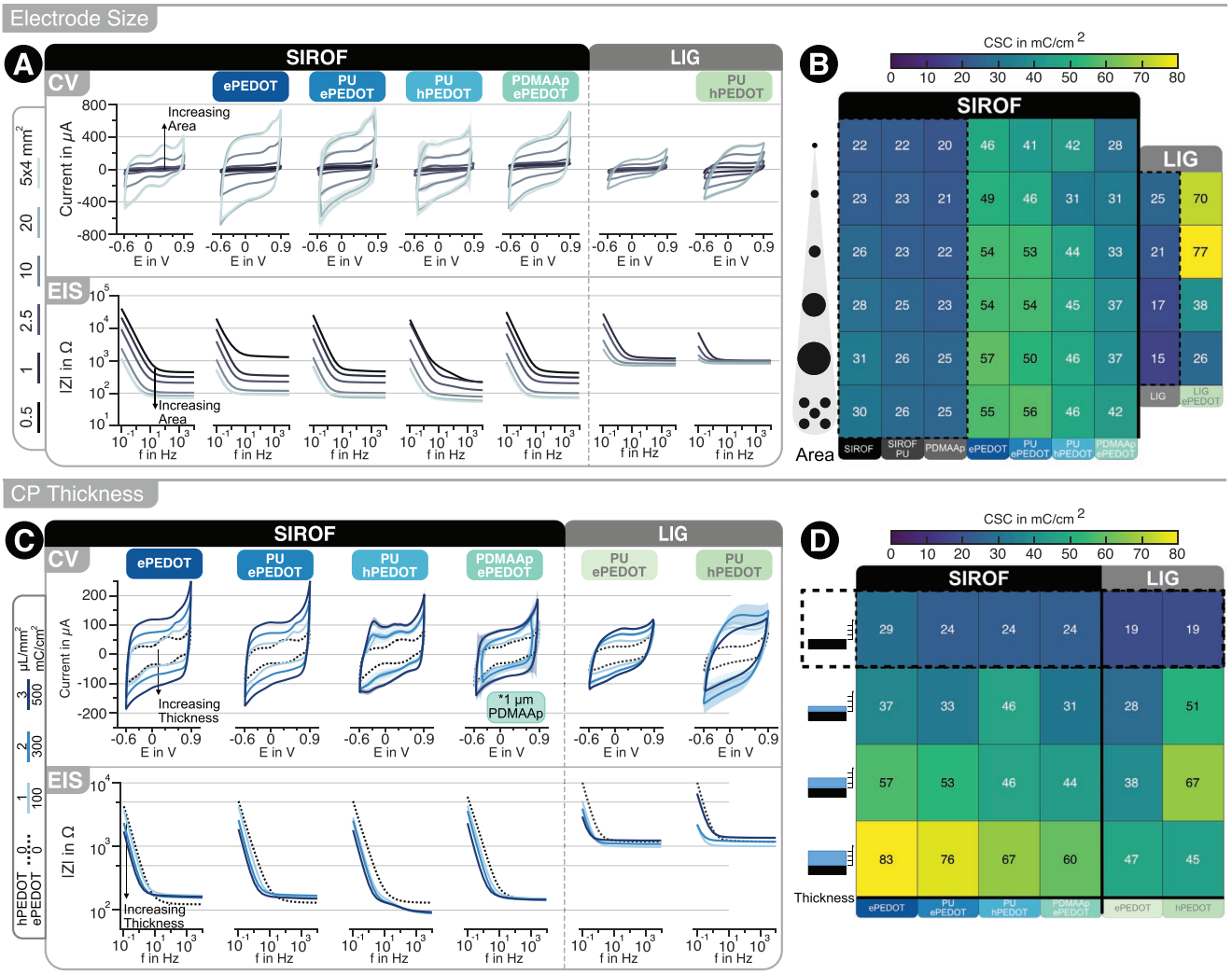


**Figure 3.** A) Comparison of CV and EIS profiles for electrodes of different active areas and CP coating (lines = mean, shade = standard deviation). B) CSC depending on electrode Area and CP (same coating thickness); dotted squares represent control, uncoated devices. C) Comparison of CV and EIS profiles for electrodes of the equal active area with varying thickness of CP coating (lines = mean, shade = standard deviation. D) CSC depending on the type of CP and its thickness (same active area); dotted square represents control, uncoated devices.

reduction of impedance when compared to uncoated LIG and SIROF, increasing the amount of current delivered during CV and reducing the impedance.

Figure 3B–D presents a graphical overview comparing the different materials and the relation between CSC, electrode area, and thickness within the respective categories. In general, the improvement of CSC through coating was more noticeable for smaller electrodes, with a two-fold increase in CSC for SIROF-based devices and almost three-fold the LIG-based ones. Control samples were furthermore included, featuring the substrate electrodes with the PU or PDMAAp functionalization but without any additional PEDOT coating. The electropolymerized ePEDOT coating of the electrodes exhibited a distinguished increase in CSC with a larger area. It was generally more reproducible than the spot-casted hPEDOT, for both SIROF and LIG-based devices (Material Section S2, Supporting Information). This is expected as the total mass of ePEDOT is directly controlled by the current during deposition. At the same time, the volume deposited during spot casting is limited by the precision of the micropipette, and the stability of the coating during annealing is limited by the lack of an insulating layer at the electrode site. Further details and the phase and Nyquist diagrams for the EIS measurements can be found on the data Section S3, Supporting Information, for all devices.

### 3.2. Stability Under Direct Current Stimulation

The ionic current delivery capability of CPs is here defined as the amount of charge that can be stored within the polymer matrix, and that is available for DCs at voltage excursions sufficiently low to not onset additional and irreversible faradaic charge transfer reactions such as water splitting. The ionic current delivery is expected to be linked to the CSC.[22,52] Increasing the volume through either expanding the surface area or increasing the

thickness of the polymer layer are both viable alternatives to increase CSC, as demonstrated by the changes in the electrode's electrochemical performance in the previous section. Thus, it is relevant to analyze how the CSC correlates with the DC stimulation performance of the different electrode coatings.

During DC stimulation, all materials and electrodes tested could sustain a 10 µA current for 2 h (72 mC) without substantial changes in current stability or electrode potential (e.g., no spikes) (**Figure 4**A). The absence of spikes indicates that the electrode surface keeps its integrity throughout the experiment

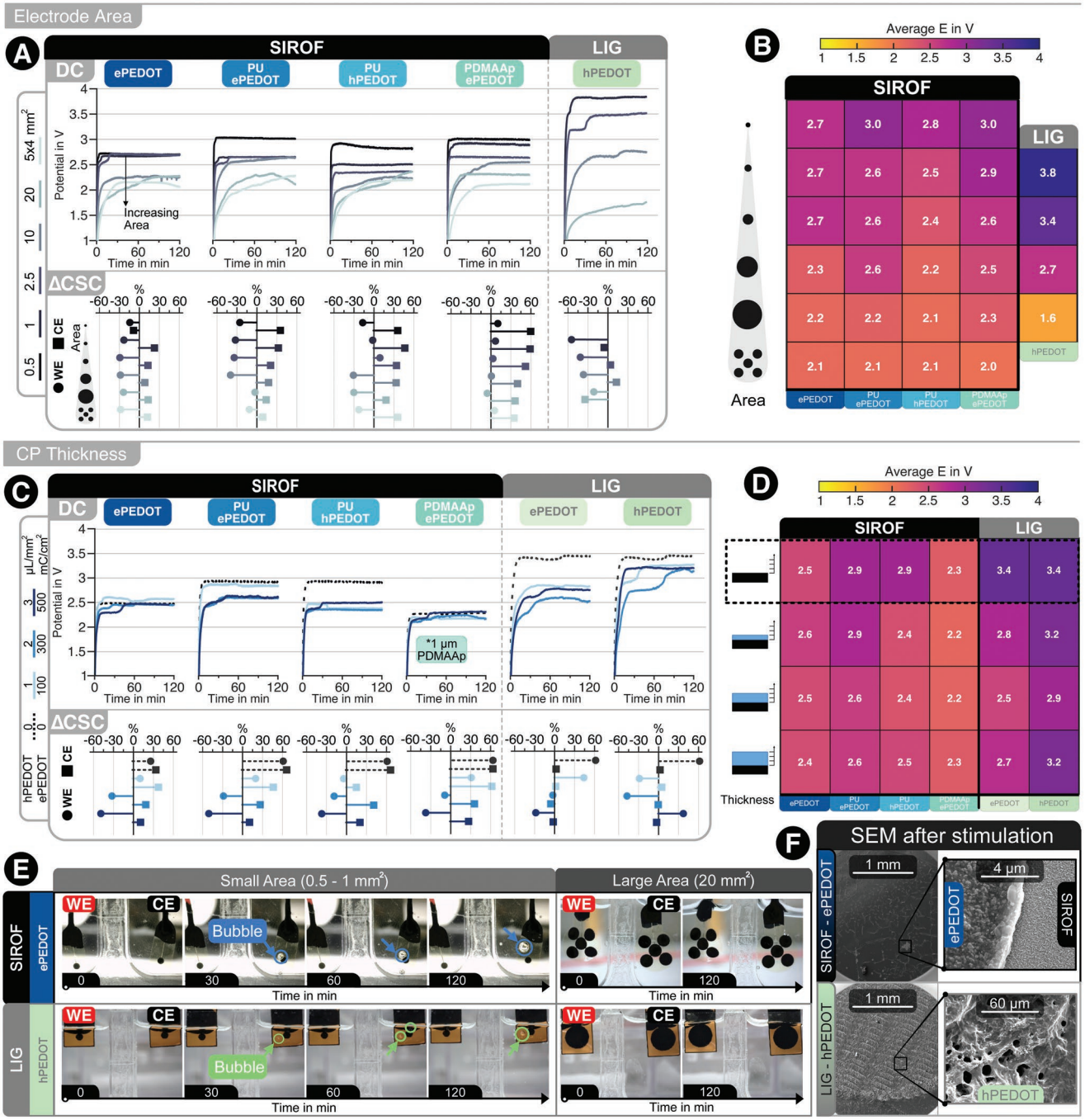


**Figure 4.** A) Cell potential measured during DC stimulation in the microfluidic chamber over 2 h at 10 µA, shown for electrodes of different areas and CP coating. Changes in CSC at the WE and CE after stimulation. B) Average cell potential for electrodes of different areas and CP coating. C) Cell potential measured during DC stimulation and changes in CSC at the WE and CE after stimulation for electrodes of different CP thicknesses ($A$ = 4 mm$^2$). D) Average cell potential for electrodes of different CP thicknesses. E) Visual inspection of electrodes during stimulation time, clear bubble formation noticeable for 1 mm$^2$ electrodes (images for other electrode sizes are found in Section S4.1 and S4.2, Supporting Information). F) SEM imaging of electrodes ($A$ = 10 mm$^2$) after DC stimulation for SIROF ePEDOT with slight damage to the CP (upper half) and LIG hPEDOT without noticeable changes in the CP (lower half) (images for other materials are found in Section S4.3, Supporting Information).

(data Section S6, Supporting Information). Typically, the electrode's potential exhibited a sharp initial increase as a step response to the applied current determined by the electrolyte resistance. After this, the potential gradually increased, reaching a state we here will refer to as the pseudo-capacitive phase, followed by a final plateau at the onset of faradaic charge transfer, where the potential remained largely constant.[53] It should be noted that the measured potential represents the sum of the voltage drop across the electrolyte and both the WE and CE. As expected, the potential needed to sustain current was reduced with increased electrode area (i.e., larger CP volume). For smaller electrodes ($A$ = 0.5 to 2.5 mm$^2$), the pseudo-capacitive phase was short, meaning that charge delivery relied mainly on faradaic current delivery. In contrast, the larger electrodes ($A$ = 10 to 20 mm$^2$) remained in the pseudo-capacitive charge delivery phase for longer before reaching the Faradaic plateau and showed, in general, no sharp potential changes. The time to reach the plateau increased with the electrode area, and the voltage at which the electrodes stabilized varied with the type of CP. This behavior was more notable with the ePEDOT and PDMAAp-ePEDOT electrodes. The other coatings (e.g., hPEDOT) never reached a stable potential (Faradaic region) within the tested time frame for large electrodes.

Immediately following DC stimulation, all electrodes were characterized through CV and EIS measurements, and their CV curves and CSC were compared against their pristine state. All electrodes changed to some extent by the stimulation, as shown by the analysis of CSC before and after stimulation (Figure 4A, lower panel). One might expect the most substantial changes to be generated at the smallest electrodes, as these experience the most extensive voltage excursions. Nevertheless, this was not confirmed by our experiments. For instance, in the case of ePEDOT on SIROF, the smallest change was seen for the smallest electrodes. Typically, one of the electrodes (WE or CE) increased its CSC while the other decreased. Which of the two electrodes increased and which one decreased varied with coating type. Importantly, and with few exceptions (i.e., the thicker CPs applied), all PEDOT electrodes, regardless of size and coating, maintained a significant part of their electroactivity, and we could not observe any immediate sign of loss of integrity of the coating (i.e., no flaking or delamination). The typical change for coated electrodes was ≈30%, except for the small PDMAAp and LIG-hPEDOT electrodes. In comparison, noncoated LIG electrodes showed the most considerable change in electroactivity of ≈60%, predominately on the WE side. These results agree with our previous findings, where we demonstrated that DCs reduces the CSC on the WE and increases it on the CE, which can be reversed through the active recharge of the electrodes using a negative current until the stimulation charge has been balanced.[16]

It is expected that voltage excursions in the range seen in Figure 4A,C (upper panels) would be sufficient to drive electrochemical reactions such as the electrolysis of water or could lead to the oxidation of saline if the voltage distribution across electrodes is not symmetric, as the expected voltage drop over the microfluidic channel should be ≈1.1 V (for the conductivity of 1.23 mS mm$^{-1}$ for PBS). Thus, our hypothesis is that once the ionic pseudo-capacitive current delivery capacity is exhausted to the point where the voltage increases and reaches a sufficient level to allow water electrolysis, this reaction will dominate any continued charge transfer. We used time-lapse imaging of the electrodes during DC stimulation to investigate if this was the case. This analysis revealed the formation of hydrogen ($H_2$) gas bubbles at the counter electrode for some electrodes (Figure 4E). This effect was noticeable for all electrodes of smaller areas (≤2.5 mm$^2$), which correlates with the larger voltage needed to drive the current of a high-impedance (i.e., small area) electrode. Furthermore, the time elapsed before the onset of $H_2$ evolution increased with electrode size. However, larger electrodes (≥10 mm$^2$) were able to prevent electrolysis (at least not visibly detected) during the 2 h of DCs. These experiments validated our hypothesis that water electrolysis is part of the DCs current. Analogous to pulsed stimulation, the total injected charge allowed must be limited and matched to the electrode size to prevent electrolysis at the electrode surface. An identifiable relationship between the dynamic changes of potential, the average stimulation potential, and the onset of electrolysis could not be identified. It should be noted that electrolysis was only noticeable at the electrode that acted as CE, or in other words, the negatively polarized electrode. In addition to time-lapse imaging, SEM analysis of the CP coatings was done on selected stimulated electrodes to visualize microscopic changes in the electrode's surface. Figure 4F shows the surface of a SIROF electrode coated with ePEDOT with microscopic fissures after stimulation and a LIG electrode coated with hPEDOT where a homogeneous coating of the porous LIG can still be observed. Though clear changes to the electrodes are noticeable, these are not directly noticeable during the stimulation timeframe. Furthermore, it should be noted, that imaging was carried out after the electrodes had been dried, and subjected to vacuum and gold sputtering, which can exacerbate the damage to the coating. (Further SEM images for other coatings are found in the data Section S4.3, Supporting Information).

A subsequent hypothesis of our study is that it would be possible to make small electrodes more potent for DCs by increasing the thickness of the coating to compensate for a smaller surface area. This would be analogous to the increased CSC with increasing thickness, as shown in Section 3.1. This hypothesis was nevertheless not confirmed by our experiments. The voltage excursion and change of CSC showed no apparent relation to "thickness," as defined by the volume of hydrogel or by polymerization charge. Thus, the area of the electrodes dictated the potential profile and average stimulation potential rather than the volume (Figure 4C). The only case where a clear trend was noticeable was for ePEDOT coatings, where thicker polymeric layers prolonged the time in which the stimulation remained in the pseudo-capacitive region before the potential reached a plateau after approximately 40 min for the thicker layer. These results indicate that even if a thicker coating inevitably will contain more ions, these, in principle, could be driven out of the electrode as ionic current water electrolysis will come to dominate charge transfer as soon as the electrode surface reaches the required potential for water electrolysis. Thus, the full ionic bulk pseudo-capacitance will contribute to the current only as long as the voltage drop over the electrode remains below the threshold for electrolysis. The electronic and ionic conductivity of the coating, which will vary depending

on the coating technique used, will determine to which extent the ionic bulk pseudo-capacitance will be able to contribute to the ionic current. In this light, it is not surprising that the electropolymerized films where the PEDOT-backbone is oriented from the electrode substrate to the electrolyte exhibit the highest electronic and ionic conductivity and, thus, the most favorable configuration for pseudo-capacitive current delivery. Furthermore, the PDMAAp electrodes are expected to show the lower potentials and smallest differences amongst coatings, as the hydrogel thickness is the same for all electrodes. Once submerged in the solution, this hydrogel is known to swell by ≈2.5 times its original thickness.

As control experiments, we also analyzed the CSC changes of uncoated electrode substrates, demonstrating that uncoated devices change drastically compared to the coated electrodes (Figure 4D). The addition of a conducting polymer influences the degree of change after stimulation, particularly for thicker layers. For all SIROF-based devices, a reduction of CSC was observed at the WE and an increase at the CE. No such relation between the CP thickness and the electrochemical change could be observed for LIG electrodes. It should be noted that no optically observable changes (i.e., discoloration, delamination, swelling) of the electrodes' surface were notable during time-lapse imaging. (Further images and graphs for all electrodes are found in the data Section S4, Supporting Information).

### 3.3. Stability Under Cyclic Load

Repeated cycling was applied to analyze the electrochemical stability of the films under cyclic load as a complement to the data on stability during DC stimulation. We analyzed the changes in both CSC and the magnitude of the electrode's impedance ($|Z|$). Results are plotted for each tested electrode after every 200 CV cycles. The total magnitude of change is represented as the percentage of change between the pristine and stressed electrodes in **Figure 5**. Observation of the changes between the new and stressed electrodes allows drawing the first conclusions about the stability of the materials and their interface during electrochemical and electromechanical stress. Still, it does not provide a complete picture of the dynamics of change. Inspecting the CSC at repeated intervals during the stress test delivers further information about the rate of change during these experiments. Furthermore, changes in the electrode impedance could be directly correlated to the changes in CSC for most of the electrodes. When the CSC increased, an apparent impedance reduction was seen at low frequencies, and an impedance increase was noticeable when CSC decreased.

All SIROF-based electrodes could withstand the repeated cycling and maintained most of their initial CSC over the entire 2000 cycles analyzed, some even increasing their CSC. ePEDOT electrodes (Figure 5A) followed a typical behavior with a sharp increase in CSC after 200 cycles (presumably related to swelling of the electrode increasing its permeability to the electrolyte) followed by a progressive decline in CSC over the subsequent 1800 cycles. ePEDOT coatings retained a significant part of their electroactivity even over 2000 CV cycles, with smaller electrodes ($A \leq 2.5$ mm$^2$) losing ≈ –15% of their CSC and larger electrodes ($A \geq 10$ mm$^2$) instead increasing their CSC by up to +3%. The use of PU as an adhesion promoter for ePEDOT reduced the variability in CSC for all electrodes tested. This is particularly notable for smaller electrodes, where the magnitude of change was approximately 10% smaller than without PU (Figure 5B). Electrodeposited PEDOT coatings on small electrodes ($A \leq 10$ mm$^2$) increased their impedance between 9% and 40% without an adhesion promoter and only between 2% and 9% with the previous coating of PU. This indicates that the adhesion promoter indeed stabilized the film as was also intended. For electrodes of 20 mm$^2$, a decrease in impedance could be noticed, with the devices of split area showing the lowest degree of change. The use of PU adhesion promoter had the same effect on the impedance as it did on the CSC, improving the stability of the coatings. In contrast to ePEDOT, hydrogel-coated SIROF electrodes showed an increase in CSC for hPEDOT and PDMAAp coatings, with an increment between +5% and +19% for the former and +15% to +31% for the latter. The two hydrogel materials differed in their characteristics over time. The CSC of hPEDOT increased sharply after the initial 200 cycles, followed by a reduction until ≈1000 cycles and then a slow increase which continued until the end of the experiment. For PDMAAp, the CSC increased consistently over the entire cycling time.

In summary, the coated SIROF electrodes endured 2000 cycles, which is a testament to the high stability of the electrodes. The total stability of these electrodes is a combination of the stability of the conducting polymer itself, the stability of the conducting substrate, and the strong bond formed between the two. Our experiments do not fully allow us to explain why some electrodes even increase their CSC with continuous cycling. A tentative explanation could be the conducting polymer's swelling, increasing the electrolyte's permeability. Alternatively, changes in the SIROF substrate itself could contribute to the increased electroactivity of the PEDOT–SIROF complex. SIROF is, in itself, porous, and the bulk of the porous film can undergo many reactions with oxygen and water, which likely also change the internal reactivity and volume of the film.[54] Although we did not explicitly investigate which reactions may be active here, it is unsurprising that this would influence the CSC. Indeed, bare SIROF electrodes continuously increased their CSC with changes between +45% and +59%, while their impedance was reduced between –50% for small electrodes ($A = 0.5$ mm$^2$) and –33% for the largest electrodes. The uncoated SIROF electrodes not only showed the most prominent difference after the stress test, but the slope of the curves during the experiment indicates that further stressing could lead to a further change in their CSC.[55]

In contrast to the stable performance of the SIROF-supported coatings, LIG-hPEDOT electrodes exhibited significant changes during cycling. LIG electrodes without any coating showed an increasing CSC during the test, with a lower magnitude of change for larger electrodes ranging between +30% and +5%. It should be noted that the smallest design completely delaminated, wherefore its data is pointed out as an outlier. For the coated electrodes, the ones with the largest area did not display a significant change in CSC. The smaller 1 mm$^2$ electrodes had a –66% reduction of CSC, while the larger 20 mm$^2$ only changed by –0.76% compared to the original state. The substantial change of CSC indicates that the CP on the small

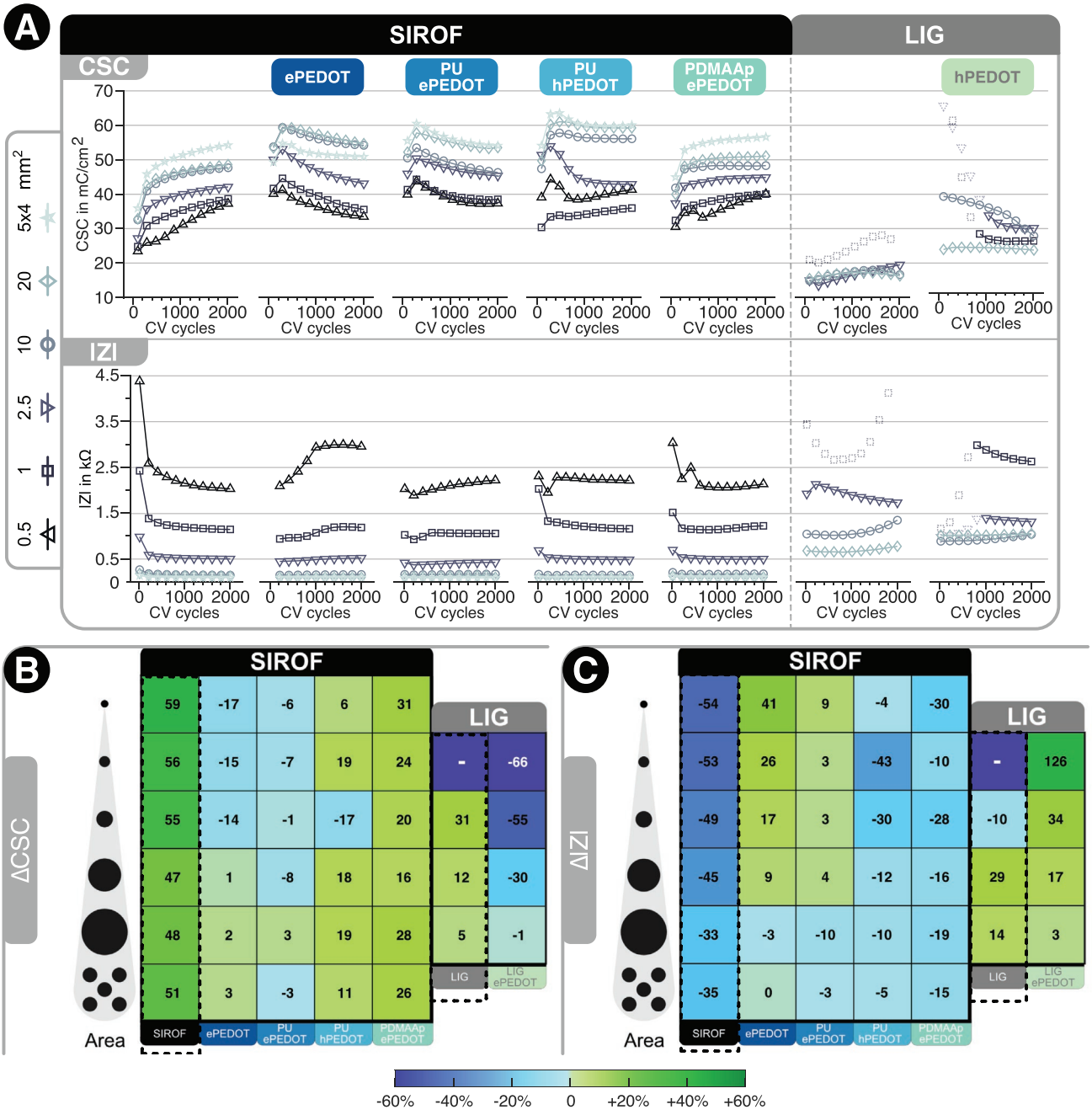


**Figure 5.** A) Changes in charge storage capacity (CSC) and electrode impedance (Z) at 1 Hz frequency throughout 2000 CV cycles, comparison of different materials, and electrode's surface area. (Dotted points represent outliers where electrodes were affected by fabrication limitations) B) Change in CSC between the pristine and stressed state in percent. C) Change in Impedance at 1 Hz between the pristine and stressed state in percent.

LIG electrodes was changing during the cyclic stressing, noticeable as the flaking of the hPEDOT layer during the initial cycles (Figure 5A, dotted points). This can be attributed to difficulties during the coating process with minimal volumes of PEDOT:PSS/DMSO solution in the current state of our protocol. Manual application of a minimal volume of hydrogel precursor (1 µl) onto a 1 $mm^2$ area without proper insulation resulted in an undefined coating surface onto which the spot-casted hydrogel could overflow and anneal not only on the desired active LIG electrode but on the bottom Kapton layer as well. For these electrodes, the smallest ones were those with a higher degree of change, with some electrodes increasing their impedance up to 125%. Larger LIG electrodes with hPEDOT showed better performance from the start as the coating process is more straightforward on larger areas, and no overflow of the CP onto the Kapton was observed, ensuring strong bonds between the underlying LIG and the CP coating stronger. All experimental results, including CVs, CSC, Impedance, Phase, and Nyquist diagrams for each tested material during the 2000 CV cycles, can be found in the supplementary data (S5).

## 4. Discussion

Conducting polymers (CPs) have been extensively researched in bioelectronic medicine in the last decades with the aim to reduce electrodes' impedance and allow for better, more reliable, long-lasting neural recording and stimulation.[20,28,29,56,57] Additionally, the capability of conductive polymers to store and deliver drugs has been of great interest in the search to reduce the inflammatory response associated with the implantation of electrodes.[58–61] However, the implementation of CPs for direct current stimulation (DCs) has not been thoroughly studied until now. The restrictions imposed on the amount of charge delivered by implantable devices and the inherent limitations of metals to be used for DCs have hindered this promising stimulation paradigm from being implemented at a larger scale and beyond more simplistic in vitro experiments. There is, nonetheless, a tangible need and interest for better materials to be used with DC stimulation. This would facilitate research on several biological processes, which rely on constant electric fields/currents, such as cell migration,[62–64] neuronal growth,[65,66] wound healing,[67–69] cancer metastasis,[70–72] and pain suppression.[73–75] In the current state-of-the-art, the implementation of DCs still relies on metal electrodes and agar bridges as electrochemical buffers. Even though several research groups have managed to miniaturize and innovate the stimulation setup,[76,77] few groups address the persistent need for electrode materials that allow DCs to be applied directly in tissue. In this context, using CPs is a new approach with promising prospects for generating constant current stimulation in biocompatible processes. This implies that additional buffering layers (i.e., agar bridges filtering the toxic metal ions eluted by Ag/AgCl) would not be needed in the future, which would facilitate the use of DCs in non-invasive applications and is an absolute prerequisite for using exogenous DCs invasively.

A key aspect of materials engineering is to weigh on the one hand, the complexity and cost of preparation and, on the other hand, the precision and performance of the resulting device. Our previous work demonstrated that electropolymerized PEDOT/PSS coatings stabilized on SIROF electrodes can deliver constant currents of sufficient magnitude to drive the movement of cancerous cells in a microfluidic channel (i.e., electrotaxis) without the need for electrochemical buffers.[16] Furthermore, we have proven that the charge depleted from the electrodes through DCs can be recuperated from the surrounding electrolyte through a recharge phase at lower currents and longer times without disturbing the cells under investigation. Based on these findings, this manuscript's framework was established to investigate further the capabilities of PEDOT-based CPs for delivering DCs at biologically relevant levels. A thorough testing protocol for the characterization of electrodes intended for DCs was developed, which provided an understandable comparison across a broad spectrum of parameters. The influence of substrate material, conducting polymer coating technology, implementation of adhesion promoters, electrode size, and polymeric thickness were cross-examined to understand how each influences DC stimulation and electrochemical stability. The current magnitude and time for DC stimulation were set with their application for electrotaxis experiments in mind. These experiments are typically carried out in precise microfluidic channels, thus achieving the desired EF strength at low currents. The use of different electrode areas at the same current magnitude permits direct assessment of the current density on the coating's stability, which has a similar effect as increasing the current for a single electrode geometry. The typical values employed for electrotaxis research are widely variable and usually not reported homogeneously.[78] Furthermore, the timeframe required for cells to sense and react to EFs varies greatly and no standardized procedure to determine these values exists to date.[69,79] Stimulation for 2 h is sufficient to elicit electrotaxis of most cells in culture and to drive all the materials tested herein into the Faradaic charge delivery range.[78] The obtained results can be extrapolated to any desired application of DCs for research and healthcare purposes.

The choice of electrode substrate is decisive for the stability of the added CP coating. It has previously been shown that smooth electrode materials (e.g., platinum) do not provide sufficient mechanical adhesion for CPs; wherefore, the electrode/polymer interface is the main failure point during stimulation.[39,80] DC signals allow electrolytes to diffuse through the polymer coating, and detrimental reactions at the substrate may, over time, undermine the CP coating. The roughness of the SIROF and LIG electrodes was not measured in this study, but we would rather expect that changes in both are related to reactions within the bulk. Therefore, it is vital also to consider the substrate's electrochemistry. Porous electrode materials such as SIROF and LIG serve a double purpose as adhesion promoters and stable stimulation electrodes once the CP coating has been depleted of ions. During testing, both electrode materials proved equally effective and durable as a substrate for CPs for DCs. Still, they showed significant differences under cyclic stressing, as clear changes in the CP coating on LIG electrodes were noticeable during the initial cycles of this test. After any unbound polymer was lost through the constant cycling process, these electrodes showed very stable properties for the remaining duration of the test (Figure 5A). Hydrogel-based PEDOT:PSS on LIG electrodes proved more durable than SIROF-stabilized electrodes for DCs, particularly for larger electrode areas (Figure 4A,B). Furthermore, the uncoated electrode materials were stable throughout electrochemical stress testing, where both showed an increment of their current delivery capabilities and CSC with repeated CV cycling. Although not further explored here, this can be attributed to the exchange and absorption of oxygen and water molecules into the iridium oxide lattice.[81] In contrast, the changes in LIG could be due to defect formation on the graphitic lattice due to oxidation or hydration of the carbon atoms.[82,83]

Inspection of the electrode's surface after stimulation through SEM showed that the coatings were different from their pristine state after DCs. These changes can be attributed to both the stress induced on the CPs through the continuous electrochemical reactions required for DCs and the mechanical changes caused by the drying of the CPs and the imaging technique. Nonetheless, the notable changes were not directly reflected on the DCs profile for any electrode, which further substantiates our hypothesis, that the outstanding capability of these electrodes to sustain DCs is a combination

**Table 2.** Comparison of advantages and compromises between the different substrate and coating materials tested.

| | Material | Advantages | Compromises |
|---|---|---|---|
| Substrate | **LIG** (Laser-Induced Graphene) | Rapid design iteration<br>Fast fabrication process<br>Low-cost equipment ($CO_2$ laser engraver) | Electrical insulation<br>Exposed electrode edges<br>Electrical connection relies on clamping methods.<br>Minimal size constrained by the laser spot size |
| | **SIROF** (Sputtered Iridium Oxide Films) | Batch fabrication at wafer level<br>Precise determination of active area at µm scale<br>Reliable electrical insulation and interconnection<br>Suitable for external and implantable devices | High-cost equipment and materials<br>Clean room and sputtering machine needed<br>Slow design iteration |
| Conducting polymer | **ePEDOT** (Electropolymerized PEDOT/PSS) | Precise deposition location and thickness<br>Excellent connection to porous substrates<br>Proven biocompatibility in implantable devices<br>Suitable for any electrode size<br>Suitable for drug delivery | Potentiostat needed<br>Devices must be coated one by one<br>Thicker layers require longer times |
| | **hPEDOT** (Spot-casted PEDOT:PSS-DMSO hydrogel) | Simple procedure<br>Easy to scale-up<br>Greater conductivity | Reproducibility of coating*<br>Thicker layers do not improve conductivity* |
| | **PDMAAp-ePEDOT** (UV-crosslinked PDMAAp hydrogel + electropolymerized PEDOT/PSS) | Wafer-level hydrogel coating possible<br>High precision of coating through UV-crosslinking<br>Proven biocompatibility and drug delivery capacity | Time-consuming<br>Galvanostat needed<br>Long polymerization times of PEDOT/PSS |

*With the current protocol

of the substrates' and CPs' electrochemical properties. Additional mechanical testing in a wet and dry state is needed to fully understand the effect of the electrochemical and mechanical stress on the CP coating during DCs, however, previous publications have demonstrated the resilience of the tested coatings to mechanical and chemical stress. We do not expect mechanical stability to be a limitation to DCs as hPEDOT on LIG can sustain at least 1000 bending cycles (±45°) in the wet state without significant changes in its electrochemical properties (CV and CSC)[84]; ePEDOT on SIROF can sustain at least 10 000 CV cycles and has a proven long-term stability with minimal changes in its impedance of at least 1.5 years in a wet environment at a temperature of 37 °C verified through accelerated aging[40]; PDMAAp on SIROF is capable of delivering at least 138 million AC pulses of 0.5 mC $cm^{-2}$ and does not change its electrochemical properties (CSC, impedance) even after 361 days in PBS at 37 °C and 5% $CO_2$, thus demonstrating long-term stability.[48]

There are clear advantages and compromises for each material when deciding the most suitable for the desired application, as listed in **Table 2**. SIROF electrodes have been well-established for several biomedical applications, allowing precision on the micrometer scale and batch fabrication in a clean room environment. However, the costs associated with the materials and machinery required for their fabrication are a limiting factor for broader use. It is hard to imagine cheap and disposable bioelectronics based on noble metals. On the other hand, LIG electrodes proved to be fast to fabricate and permit rapid iteration of electrode design, limited only by the minimal electrode dimensions possible with the chosen fabrication approach. These limitations can be overcome through variations in the lasering process and by using different substrate materials, as shown by Li et.al.[85] The electrochemical properties of CP coatings on LIG electrodes were stable and comparable to those on SIROF. The low-cost fabrication and rapid design iteration permitted by these devices make them a great alternative to standard metal-based electrodes and provide a suitable platform for experimentation.

With the advantages and compromises of each material in mind, we decided to compare different polymerization techniques in combination with different adhesion promotion approaches within our DCs and cyclic stress protocol to investigate and determine the best material combination. The conducting polymers and hydrogels chosen for this study are meant to represent chemically similar materials (PEDOT and SS being the common denominators) but, at the same time, opposite spectrums of possible coating strategies. Additional analysis and fine-tuning of the chemical synthesis and coating strategy of these CPs could further improve their DCs properties and stability, as the specific chemistry strongly influences both the electrical and mechanical properties of CPs. All the materials tested herein proved suitable for delivering direct current with subtle but clear advantages and disadvantages between the different coatings. Electropolymerized PEDOT/PSS (ePEDOT) demonstrated the highest charge storage capacities, was the second most stable CP during DC stimulation and outperformed any other material during repeated electrochemical stress. The high performance of ePEDOT is attributed to its high electronic and ionic conductivity, the use of a large, immobilized dopant PSS, the precise coating within the active electrode site through electropolymerization, and its superior adhesion to SIROF substrates, which mechanically stabilizes the film. The use of a polyurethane-based (PU) adhesion promoter showed a slight improvement in the mechanical and electrical stability of ePEDOT on SIROF electrodes during stimulation; however, the increase in fabrication complexity is unreturned for these electrodes. This was particularly noteworthy for small electrodes ($A < 10$ $mm^2$), where the electrode geometry hindered the flow

of PU within the electrode cavity during the dip-coating process and, with most certainty, led to an increase in the PU thickness, which had an insulating effect.[43] Using a PDMAAp hydrogel matrix into which PEDOT could be electrochemically grown was intended to improve the electrochemical properties of the electrode by providing a larger volume for ions to be stored and lower diffusion resistance. This material combination had previously been studied for its use in neural stimulation and recording showing promising results.[29,48,61] The entrapment of SSNa ions within the hydrogel matrix forces PEDOT polymeric chains to grow along the charged backbone of the hydrogel. The concentration of dopant used for this research (2.5%) proved insufficient to improve the electrical performance of the electrodes significantly. Nonetheless, the thick hydrogel layer (≈1 µm) and its swelling properties in water provided a large volume to store ions leading to lower potentials for these electrodes in comparison to the other CPs, particularly for the largest electrodes with a split area ($A$ = 20 mm$^2$) and for all experiments with varied CP thickness (Figure 4B,D). Further research on the synthesis of hydrogels with higher dopant concentrations could lead to significant improvement of this material combination.

Coating electrodes with pure PEDOT:PSS hydrogels (hPEDOT) provide a cost and time-efficient alternative to ePEDOT, particularly for the functionalization of macro-electrodes. The previously established coating protocol facilitates the parallelization of electrode preparation.[84] It is repeatable and reliable for electrodes with a larger active area ($A \geq 10$ mm$^2$), as demonstrated by the stability of the coating after repeated cycling and DC stimulation. Smaller hPEDOT electrodes were more prone to failure during experiments. They were outperformed by the other materials, which may not fully reflect on the type of material but more on the limitations of the coating technique itself. The simple coating method applied in this study (i.e., spot-casting) was limited in terms of its capability to obtain a conformal and reproducible coating, which makes it difficult to compare these electrodes to their electrodeposited counterparts directly. Homogeneous electrode coating with hPEDOT significantly improved their DCs properties on both SIROF and LIG substrates. This can be attributed to the use of DMSO during hydrogel preparation, which enhances cohesion between PEDOT molecules, generating interconnected PEDOT-rich regions within the polymer that allow for efficient electron transport.[45,86] Recent advancements in 3D printing of similar hydrogels demonstrate that these limitations can be overcome to make the coating of small electrodes more reliable.[87]

All materials tested here have their respective advantages and compromises in different scenarios and combinations. Therefore, we suggest improvements to the underlying electrode and the CP coatings in **Table 3**. There are several publications on each of these materials where the coating methods and electrochemical properties have been investigated individually, particularly for their use as recording or stimulation electrodes utilizing alternating currents. The research of their DCs properties opens a new frontier for bioelectronic medicine, thanks to the outstanding charge storage capacity of these PEDOT-based CPs, their ionic pseudo-capacitive charge delivery capabilities, and demonstrated DCs stability. With these results, we aim to provide the initial step towards the further investigation of DCs as a stimulation paradigm with conducting polymer electrodes optimized for this purpose, wherefore, a comprehensive comparison of all materials tested alongside proposed use cases is provided.

To create a fair and meaningful comparison among the tested materials, we developed a visual representation of different weighted parameters that showcases each coating's advantages and drawbacks, taking both electrochemical performance and the preparatory procedure into account. Fabrication efficiency relates to the percentage of active user time required during the coating process. A higher value equals longer active time, which directly increases the human resources needed for a particular type of material. The simplicity of fabrication measures the number of steps and processes for successful CP coating. More steps increase the probability of human error and make the process less accessible to inexperienced people. The CSC is a proxy for the expected electrochemical performance since higher values lead to higher currents at lower potentials, thus

**Table 3.** Proposed improvements to the different materials.

| | Material | Proposed improvements | Reason |
|---|---|---|---|
| Substrate | **LIG** (Laser-Induced Graphene) | Use of insulation layer with precise electrode openings | Prevent unwanted current flow through tracks and provide precise electrode area for stimulation |
| | **SIROF** (Sputtered Iridium Oxide Films) | Pre-conditioning of the material | Improvement of charge storage capacity and reduction of impedance |
| Conducting polymer | **ePEDOT** (electropolymerized PEDOT/PSS) | Scaled fabrication method | Parallelization of the coating procedure for several electrodes can reduce time and costs |
| | **hPEDOT** (spot-cast PEDOT:PSS-DMSO hydrogel) | Use of a more viscose/higher PEDOT:PSS density formulation<br>Use of screen printing or CNC machine for spot casting | Ensure that the hydrogel stays on the active electrode surface<br>Reduce time and improve the quality of coatings |
| | **PDMAAp-ePEDOT** (UV-crosslinked PDMAAp hydrogel + electropolymerized PEDOT/PSS) | Use of a higher percentage of NaPSS in the hydrogel<br>Cross-linking in the swollen state | Improve integration of ePEDOT during electropolymerization and increase charge storage capacity<br>Prevent extreme swelling after submersion in water, particularly for small electrodes |

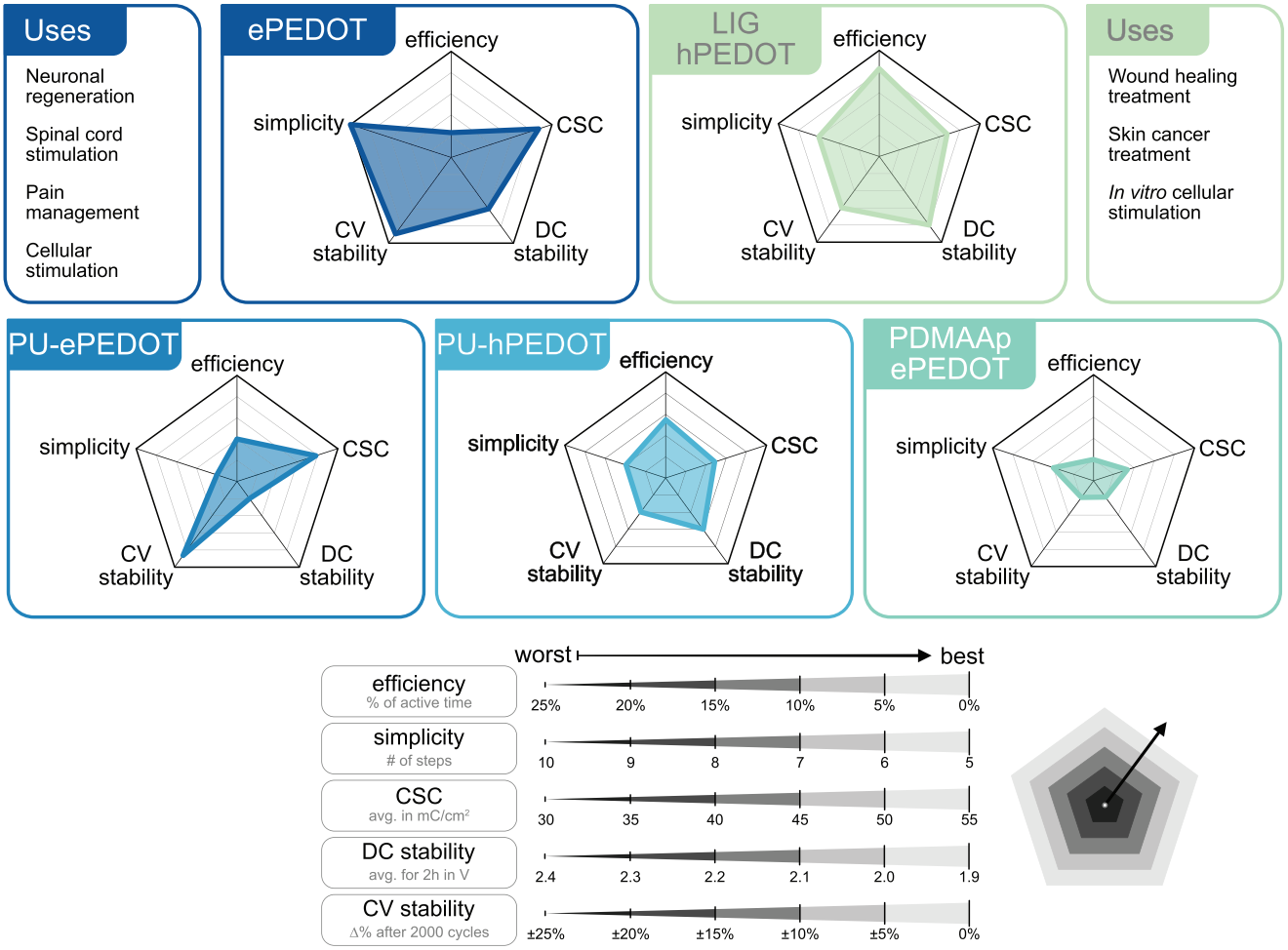


**Figure 6.** Comparison of the most relevant properties (efficiency, simplicity, CSC, DC, and CV stability) for choosing a particular combination of electrode material and conducting polymer. Proposed use cases for electropolymerized PEDOT on SIROF and spot-cast hydrogel hPEDOT on LIG.

ensuring longer pseudo-capacitive charge delivery. Drawing from the experimental results, the DC and CV stability of the electrodes were chosen as the final significant values for analysis. The DC stability is calculated as the mean cell potential after the initial capacitive discharge (10 min), which is lower for materials with longer pseudo-capacitive charge delivery times. Lower potentials are also associated with the absence of noticeable electrolysis during DCs. Finally, CV stability is calculated by the CSC change percentage during cyclic loading. A higher degree of change (reduction or increase) is related to the lower stability of the electrode coating; therefore, a lower percentage is desired. A graphic representation of these parameters (**Figure 6**) is intended as a practical guide for choosing a specific conducting polymer or hydrogel for the desired implementation of DC stimulation.

The wide range of possible materials provides an exciting and promising future for the application of DCs in implantable and external electroceuticals for wound healing, cancer therapy, nerve restoration, pain management, and much more. The use of novel hydrogels that can be UV-crosslinked on miniaturized electrodes in combination with potential-future drug-delivery properties can open a new realm for implantable DC stimulation[61] while the spot casting of PEDOT:PSS hydrogels on cost-effective, relatively simple LIG electrodes can pave the way towards the future of external bioelectronics.

## 5. Conclusion

All the investigated materials herein can be used for stable DCs for up to 2 h with relatively large electrodes ($A \geq 10$ mm$^2$) and sustain cyclic loading of up to 2000 CV cycles without complete failure. The use of DCs as a stimulation paradigm in combination with micro-electrodes still requires fine-tuning of the chemical properties of each CP, the coating technique employed, and the adhesion between substrate and polymer. After careful analysis of the obtained results and the different ways the devices can be functionalized, we can confidently provide a comprehensive comparison of the most relevant parameters one has to consider when choosing between these PEDOT-based CPs. Furthermore, the data presented in this work allows a deeper analysis of the underlying electrochemical processes involved in the charge delivery process during DCs with the tested materials.

Our initial hypothesis for the mechanism of charge delivery during DCs for CPs relied on the assumption that, as long as the ions within the polymeric matrix have not been depleted, the current flow should happen through pseudo-capacitive reactions. The electrode-electrolyte interface can be simplified through an equivalent electrical circuit consisting of a double-layer capacitance $C_{DL}$ in parallel to a Warburg impedance $Z_W$ and a Faradaic resistance $R_F$ all in series to the electrolyte access resistance $R_A$. This circuit entails that the voltage response to an applied direct current should be the rapid charging of $C_{DL}$, followed by a plateau at the onset of Faradaic surface reactions with very low involvement of the Warburg element, as diffusion is not a limiting factor in the Faradaic region (**Figure 7**A). Suppose a noble-metal electrode is used (e.g., platinum, iridium

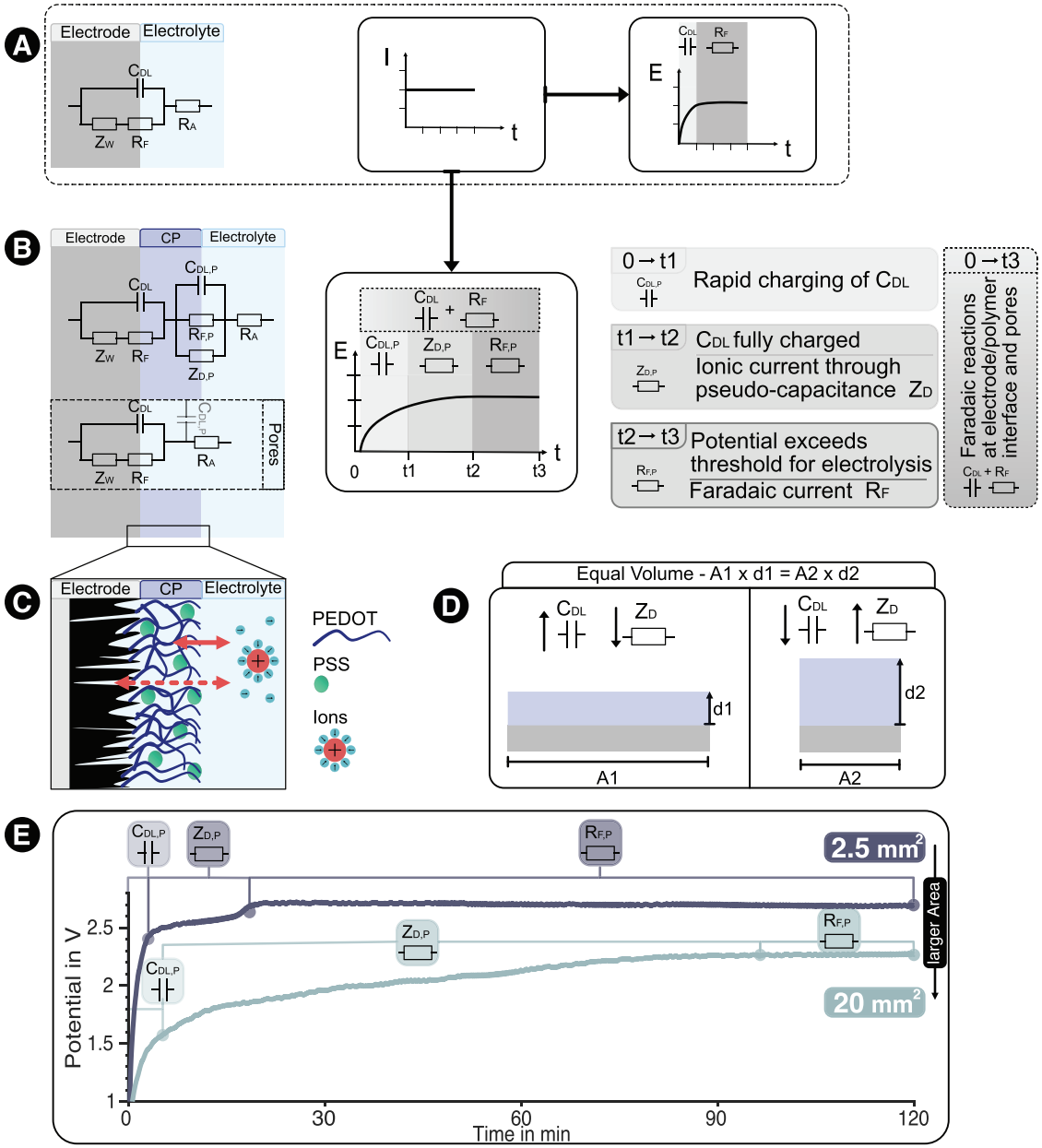


**Figure 7.** A) equivalent circuit of the electrode-electrolyte interface of noble-metal electrodes with access resistance ($R_A$), Faradaic resistance ($R_F$), Warburg impedance ($Z_w$), and double layer capacitor ($C_{DL}$). Expected electrode potential during DCs with initial capacitive charge delivery followed by Faradaic reactions. B) proposed equivalent circuits for CPs on rough materials with Faradaic resistance ($R_{F,P}$), diffusion impedance ($Z_{D,P}$) and double layer capacitor ($C_{DL,P}$). Representation of equivalent circuit within pores (dotted square). Expected electrode potential during DCs with the extended pseudo-capacitive region and possible parallel reactions. C) Schematic representation of polymer on a rough substrate with possible diffusion pathways for ions and water molecules. D) Schematic representation of expected changes to diffusion impedance ($Z_{D,P}$) and double layer capacitor ($C_{DL,P}$) for electrodes of the same volume but different areas and thicknesses. E) Potential curves for SIROF electrodes of a different area with 300 mC cm$^{-2}$ ePEDOT coatings. Different charge delivery regions are marked respectively to exemplify the influence of CP volume on the different charge delivery mechanisms of the proposed model.

oxide). In that case, this assumption holds, and the potential is high enough for the onset of electrolysis at the interface, followed by immediate damage to the electrode (Section S6, Supporting Information).

For the electrodes investigated herein, this model does not suffice to explain the observed behavior, as electrodes can deliver DCs for extended periods without reaching the Faradaic plateau in some cases (i.e., large areas). Furthermore, even when rough electrodes (i.e., SIROF, LIG) coated with the PEDOT-based CPs developed electrolytic reactions (i.e., hydrogen evolution), complete loss of the CP coating or damage to the underlying electrode was not observed, in contrast to metal electrodes (Sections S6 and S7, Supporting Information). Several electrical models based on EIS measurements exist to explain the influence of porous electrodes and CPs on electrode impedance and charge transfer.[50,88–95] However, these models are not suitable for describing electrochemical reactions during DCs, as the signal used for impedance measurements is always of alternating current at frequencies above zero and low potentials.

Therefore, we propose an alternative equivalent circuit encompassing all charge delivery mechanisms happening in parallel during DCs with these polymers. Our model considers the metal-polymer interface and the presence of pores within the polymeric matrix and the rough substrate. The electronic model stated before remains unchanged for the underlying electrode, and is connected in series to the polymeric chains, which can be modeled as a double-layer capacitor $C_{DL,P}$, a diffusion impedance $Z_D$ and a Faradaic Resistance $R_{F,P}$, all in parallel as depicted in Figure 7B. These electronic components represent the complex electrochemical reactions happening at the CP layer and have, hence, not a fixed value, changing over time as the charge passes through the coating. During the first moments of stimulation, the potential increases exponentially following the charging of $C_{DL,P}$, which represents the initial movement of ions at the polymer-electrolyte interface. Once this purely capacitive reaction is in balance, ions within the polymeric matrix are forced in or out of the CP due to electrostatic interaction with the polymeric chains and dopant ions. This pseudo-capacitive reaction is represented by $Z_D$, which has an initial low value that increases as the electronic balance within the polymer changes with the movement of charge.

It should be noted that different charge carriers diffuse within the polymer at different rates, and water molecules move in and out of the polymer, leading to the expansion/shrinkage of the CP.[86,96–99] The time at which each electrode delivers charge in a pseudo-capacitive manner varies with electrode area and polymer thickness, as the diffusion length and overall volume change. Once the potential at $Z_D$ reaches the water window (i.e., –0.6 or +0.9 V), charge delivery becomes dominated by purely Faradaic electrolytic surface processes ($R_{F,P}$), and the influence of $C_{DL,P}$, and $Z_D$ is negligible, leading to a plateau in the potential-time curve. These reactions are only one part of the story, as CPs and the employed electrodes are porous, wherefore water molecules from the solution can move freely within the pores in the polymer and reach the underlying substrate at which different electrochemical reactions can take place as previously explained (Figure 7C). Furthermore, an inhomogeneous coating thickness could lead to uneven potential distribution and the parallel onset of all charge delivery mechanisms throughout the electrode area. The electrochemical evaluation of this hypothesis falls beyond the scope of the paper, however, initial tests driving the electrodes at potentials above the water window clearly demonstrate that electrolysis takes place at the platinum-SIROF interface leading to complete delamination of the SIROF and PEDOT/PSS coating, thus proving that all reactions can happen in parallel (Supplementary S9).

Nonetheless, the data presented herein provide significant evidence of our proposed model. This model could also explain the observed behavior of electrodes with thick polymeric coatings. There, the current delivery was mainly dominated by faradaic reactions, and sharp changes in the potential could be observed. A larger electrode area leads to a higher $C_{DL,P}$, and a lower $Z_D$; therefore, large electrodes remain within the pseudo-capacitive charge delivery region for longer. In contrast, a small electrode area with a thick CP to achieve the same volume results in a lower $C_{DL,P}$, and a higher $Z_D$, which results in a shorter pseudo-capacitive charge delivery phase (Figure 7D).

To summarize, the electrodes tested herein are not exempt from forming chemical by-products and pH changes that might be generated during stimulation. Thus, if constant pH is required for the application, it is crucial to balance the stimulation current density and duration to minimize this effect. Nonetheless, careful analysis of the electrode potential variations in combination with the buffering capacity of biological fluids could mitigate these adverse effects. Observation of the different electrodes of varying size and material combinations shows the influence of each variable on the charge delivery mechanisms, which allows the determination of the most suitable material combination depending on the desired application of DCs. We firmly believe that the combination of several electrochemical mechanisms for charge delivery is the reason for the outstanding DCs performance of the materials presented herein. This work is the first step toward the broader implementation of CPs for DCs applications.

## Supporting Information

Supporting Information is available from the Wiley Online Library or from the author.

## Acknowledgements

This project was funded by the European Research Council (ERC) under the European Union's Horizon 2020 Research and Innovation program under a grant agreement (No. 759655, SPEEDER). This work furthermore received support from BrainLinks-BrainTools, Cluster of Excellence funded by the German Research Foundation (DFG, EXC 1086), currently funded by the Federal Ministry of Economics, Science and Arts of Baden Württemberg within the sustainability program for projects of the excellence initiative. Additionally, the authors would like to acknowledge the support of the Freiburg Institute for Advanced Studies FRIAS. The authors would also like to acknowledge the support of Prof. Dr. Jürgen Rühe and his team at the Laboratory for Chemistry and Physics Interfaces (CPI) at the University of Freiburg for synthesizing both the PDMAAp hydrogel and the UV-reactive silane employed in this study, as well as for providing access to their laboratories.

Open access funding enabled and organized by Projekt DEAL.

## Conflict of Interest

The authors declare no conflict of interest.

## Author Contributions

**José Leal**: conceptualization (lead), investigation (lead), data curation (lead), formal analysis (lead), visualization (lead), writing – original draft preparation (lead), writing – review & editing (equal). **Sebastian Shaner**: conceptualization (supporting), formal analysis (supporting), writing – review & editing (equal). **Lukas Matter**: writing – review & editing (equal). **Christian Böhler**: conceptualization (supporting), writing – review & editing (equal). **Maria Asplund**: conceptualization (lead), formal analysis (lead), writing – review & editing (equal).

## Data Availability Statement

The data that support the findings of this study are available from the corresponding author upon reasonable request.

## Keywords

biomaterials, conducting polymers, direct current stimulation, Carbon, PEDOT

Received: November 9, 2022
Revised: December 16, 2022
Published online:

[1] J. Rivnay, S. Inal, A. Salleo, R. M. Owens, M. Berggren, G. G. Malliaras, *Nat. Rev. Mater.* **2018**, *3*, 17086.
[2] H. Bronstein, C. B. Nielsen, B. C. Schroeder, I. McCulloch, *Nat. Rev. Chem.* **2020**, *4*, 66.
[3] J. Janata, M. Josowicz, *Nat. Mater.* **2003**, *2*, 19.
[4] Z. Shen, Z. Zhang, N. Zhang, J. Li, P. Zhou, F. Hu, Y. Rong, B. Lu, G. Gu, *Adv. Mater.* **2022**, *34*, 2203650.
[5] W. Zhang, Y. C. Wang, X. Li, C. Song, L. Wan, K. Usman, J. Fang, *Adv. Sci.* **2018**, *5*, 1800159.
[6] S. Lu, Y. Sun, K. Ren, K. Liu, Z. Wang, S. Qu, *Polymers* **2018**, *10*, 5.
[7] R. Po, C. Carbonera, A. Bernardi, F. Tinti, N. Camaioni, *Sol. Energy Mater. Sol. Cells* **2012**, *100*, 97.
[8] H. Liu, M. Li, R. B. Kaner, S. Chen, Q. Pei, *ACS Appl. Mater. Interfaces* **2018**, *10*, 15609.
[9] S. I. Na, G. Wang, S. S. Kim, T. W. Kim, S. H. Oh, B. K. Yu, T. Lee, D. Y. Kim, *J. Mater. Chem.* **2009**, *19*, 9045.
[10] Q. Zhao, J. Liu, Z. Wu, X. Xu, H. Ma, J. Hou, Q. Xu, R. Yang, K. Zhang, M. Zhang, H. Yang, *Chem. Eng. J.* **2022**, *442*, 136284.
[11] Y. Shi, L. Peng, Y. Ding, Y. Zhao, G. Yu, *Chem. Soc. Rev.* **2015**, *44*, 6684.
[12] T. S. Mathis, N. Kurra, X. Wang, D. Pinto, P. Simon, Y. Gogotsi, *Adv. Energy Mater.* **2019**, *9*, 39.
[13] X. Jia, Y. Ge, L. Shao, C. Wang, G. G. Wallace, *ACS Sustain Chem Eng* **2019**, *7*, 14321.
[14] T. Schoetz, M. Kurniawan, M. Stich, R. Peipmann, I. Efimov, A. Ispas, A. Bund, C. Ponce De Leon, M. Ueda, *J. Mater. Chem. A Mater.* **2018**, *6*, 17787.
[15] G. E. Fenoy, O. Azzaroni, W. Knoll, W. A. Marmisollé, *Chemosensors* **2021**, *9*, 212.
[16] J. Leal, N. Jedrusik, S. Shaner, C. Boehler, M. Asplund, *Biomaterials* **2021**, *275*, 120949.
[17] M. ElMahmoudy, V. F. Curto, M. Ferro, A. Hama, G. G. Malliaras, R. P. O'Connor, S. Sanaur, *J. Appl. Polym. Sci.* **2019**, *136*, 47029.
[18] D. N. Heo, S.-J. Lee, R. Timsina, X. Qiu, N. J. Castro, L. G. Zhang, *Mater. Sci. Eng., C* **2019**, *99*, 582.
[19] C. Boehler, M. Asplund, in *40th Annual International Conference of the IEEE Engineering in Medicine and Biology Society (EMBC)*, IEEE, Honolulu, HI, USA **2018**, p. 2202.
[20] S. Venkatraman, J. Hendricks, Z. A. King, A. J. Sereno, S. Richardson-burns, D. Martin, J. M. Carmena, S. Member, *IEEE Trans. Neural. Syst. Rehabil. Eng.* **2011**, *19*, 307.
[21] C. Boehler, M. Asplund, *J. Biomed. Mater. Res. A* **2015**, *103*, 1200.
[22] T. H. Le, Y. Kim, H. Yoon, *Polymers* **2017**, *9*, 150.
[23] R. Balint, N. J. Cassidy, S. H. Cartmell, *Acta Biomater.* **2014**, *10*, 2341.
[24] N. K. Guimard, N. Gomez, C. E. Schmidt, *Prog. Polym. Sci.* **2007**, *32*, 876.
[25] E. A. Kamoun, E. R. S. Kenawy, X. Chen, *J. Adv. Res.* **2017**, *8*, 217.
[26] B. D. Malhotra, A. Chaubey, S. P. Singh, *Anal. Chim. Acta* **2006**, *578*, 59.
[27] C. Baker, K. Wagner, P. Wagner, D. L. Officer, D. Mawad, *Adv. Phys. X* **2021**, *6*, 1899850.
[28] M. Asplund, T. Nyberg, O. Inganäs, *Polym. Chem.* **2010**, *1*, 1374.
[29] C. Kleber, M. Bruns, K. Lienkamp, J. Rühe, M. Asplund, *Acta Biomater.* **2017**, *58*, 365.
[30] R. A. Green, S. Baek, L. A. Poole-Warren, P. J. Martens, *Sci. Technol. Adv. Mater.* **2010**, *11*, 014107.
[31] S. F. Cogan, *Annu. Rev. Biomed. Eng.* **2008**, *10*, 275.
[32] L. b. Robblee, J. McHardy, J. M. Marston, S. B. Brummer, *Biomiaterials* **1980**, *1*, 50.
[33] T. L. Rose, L. S. Robblee, *IEEE Trans. Biomed. Eng.* **1990**, *37*, 1118.
[34] R. H. W. Funk, *Front. Physiol.* **2015**, *6*,.
[35] M. E. Hatten, *Science* **2002**, *297*, 1660.
[36] R. Nuccitelli, *Curr. Top. Dev. Biol.* **2003**, *58*, 1.
[37] N. Donaldson, P. E. K. Donaldson, *Med. Biol. Eng. Comput.* **1986**, *24*, 50.
[38] B. Song, Y. Gu, J. Pu, B. Reid, Z. Zhao, M. Zhao, *Nat. Protoc.* **2007**, *2*, 1479.
[39] C. Boehler, F. Oberueber, T. Stieglitz, M. Asplund, in *Int. IEEE/EMBS Conf. Neural Engineering NER*, Montpellier, France **2015**, p. 410.
[40] C. Boehler, F. Oberueber, S. Schlabach, T. Stieglitz, M. Asplund, *ACS Appl. Mater. Interfaces* **2017**, *9*, 189.
[41] R. Toomey, D. Freidank, J. Rühe, *Macromolecules* **2004**, *37*, 882.
[42] C. Boehler, S. Carli, L. Fadiga, T. Stieglitz, M. Asplund, *Nat. Protoc.* **2020**, *15*, 3557.
[43] A. Inoue, H. Yuk, B. Lu, X. Zhao, *Sci. Adv.* **2020**, *6*, eaay5394.
[44] B. Lu, H. Yuk, S. Lin, N. Jian, K. Qu, J. Xu, X. Zhao, *Nat. Commun.* **2019**, *10*, 1043.
[45] X. Fan, W. Nie, H. Tsai, N. Wang, H. Huang, Y. Cheng, R. Wen, L. Ma, F. Yan, Y. Xia, *Adv. Sci.* **2019**, *6*, 1900813.
[46] I. Lee, G. W. Kim, M. Yang, T. S. Kim, *ACS Appl. Mater. Interfaces* **2016**, *8*, 302.
[47] H. Yuk, B. Lu, X. Zhao, *Chem. Soc. Rev.* **2019**, *48*, 1642.
[48] C. Kleber, K. Lienkamp, J. Rühe, M. Asplund, *Adv. Biosyst.* **2019**, *3*, 1900072.
[49] O. Prucker, C. A. Naumann, J. Rühe, W. Knoll, C. W. Frank, *J. Am. Chem. Soc.* **1999**, *121*, 8766.
[50] A. R. Harris, P. J. Molino, R. M. I. Kapsa, G. M. Clark, A. G. Paolini, G. G. Wallace, *Analyst* **2015**, *140*, 3164.
[51] M. Bianchi, S. Carli, M. di Lauro, M. Prato, M. Murgia, L. Fadiga, F. Biscarini, *J. Mater. Chem. C Mater.* **2020**, *8*, 11252.
[52] F. Hu, Y. Xue, J. Xu, B. Lu, *Front. Robot. AI* **2019**, *6*, 114.
[53] E. McAdams, in *Encyclopedia of Medical Devices and Instrumentation*, John Wiley & Sons, Inc. , Hoboken, NJ, USA **2006**, p. 120.
[54] E. Slavcheva, R. Vitushinsky, W. Mokwa, U. Schnakenberg, *J. Electrochem. Soc.* **2004**, *151*, E226.
[55] O. Kasian, J.-P. Grote, S. Geiger, S. Cherevko, K. J. J. Mayrhofer, *Angew. Chem.* **2018**, *130*, 2514.

[56] E. M. Thaning, M. L. M. Asplund, T. A. Nyberg, O. W. Inganäs, H. Von Holst, *J. Biomed. Mater. Res. B Appl. Biomater.* **2010**, *93*, 407.
[57] D. Mantione, I. del Agua, A. Sanchez-Sanchez, D. Mecerreyes, *Polymers* **2017**, *9*, 354.
[58] M. R. Abidian, D. C. Martin, *Adv. Funct. Mater.* **2009**, *19*, 573.
[59] M. R. Abidian, D. C. Martin, *Biomaterials* **2008**, *29*, 1273.
[60] C. Boehler, C. Kleber, N. Martini, Y. Xie, I. Dryg, T. Stieglitz, U. G. Hofmann, M. Asplund, *Biomaterials* **2017**, *129*, 176.
[61] C. Kleber, K. Lienkamp, J. Rühe, M. Asplund, *Adv. Healthcare Mater.* **2019**, *8*, 1801488.
[62] B. Cortese, I. E. Palamà, S. D'Amone, G. Gigli, *Integr. Biol.* **2014**, *6*, 817.
[63] A. Haeger, K. Wolf, M. M. Zegers, P. Friedl, *Trends Cell Biol.* **2015**, *25*, 556.
[64] Y. S. Sun, S. W. Peng, J. Y. Cheng, *Biomicrofluidics* **2012**, *6*, 034117.
[65] M. E. Mycielska, M. B. A. Djamgoz, *J. Cell Sci.* **2004**, *117*, 1631.
[66] A. Jahanshahi, L. M. Schönfeld, E. Lemmens, S. Hendrix, Y. Temel, *Mol. Neurobiol.* **2014**, *49*, 1005.
[67] J. I. Hoare, A. M. Rajnicek, C. D. McCaig, R. N. Barker, H. M. Wilson, *J. Leukoc. Biol.* **2015**, *99*, 1141.
[68] P. E. Houghton, C. B. Kincaid, M. Lovell, K. E. Campbell, D. H. Keast, M. G. Woodbury, K. A. M. Harris, *Phys. Ther.* **2003**, *83*, 17.
[69] M. Ashrafi, T. Alonso-Rasgado, M. Baguneid, A. Bayat, *Vet. Dermatol.* **2016**, *27*, 235.
[70] Y. Li, T. Xu, X. Chen, S. Lin, M. Cho, D. Sun, M. Yang, *Anal. Bioanal. Chem.* **2017**, *409*, 2163.
[71] K. Zhu, N. R. Hum, B. Reid, Q. Sun, G. G. Loots, M. Zhao, *Sci. Rep.* **2020**, *10*, 8712.
[72] C. W. Huang, J. Y. Cheng, M. H. Yen, T. H. Young, *Biosens. Bioelectron.* **2009**, *24*, 3510.
[73] N. Bhadra, K. L. Kilgore, *IEEE Trans. Neural Syst. Rehabil. Eng.* **2004**, *12*, 313.
[74] F. Yang, M. Anderson, S. He, K. Stephens, Y. Zheng, Z. Chen, S. N. Raja, F. Aplin, Y. Guan, G. Fridman, *Sci. Adv.* **2018**, *4*, eaaq1438.
[75] T. Vrabec, N. Bhadra, G. Van Acker, N. Bhadra, K. Kilgore, *IEEE Trans. Neural Syst. Rehabil. Eng.* **2017**, *25*, 517.
[76] T. J. Zajdel, G. Shim, L. Wang, A. Rossello-Martinez, D. J. Cohen, *Cell Syst.* **2020**, *10*, 506.
[77] T. J. Zajdel, G. Shim, D. J. Cohen, *Biosens. Bioelectron.* **2021**, *192*, 113479.
[78] S. Guette-Marquet, C. Roques, A. Bergel, *Bioelectrochemistry* **2021**, *139*, 107737.
[79] S. Ud-Din, A. Bayat, *Healthcare* **2014**, *2*, 445.
[80] J. Leal, N. Jedrusik, S. Shaner, C. Boehler, M. Asplund, *Biomaterials* **2021**, *275*, 120949.
[81] L. D. Burke, D. P. Whelan, *J. Electroanal. Chem.* **1984**, *162*, 121.
[82] Y. Yi, G. Weinberg, M. Prenzel, M. Greiner, S. Heumann, S. Becker, R. Schlögl, *Catal. Today* **2017**, *295*, 32.
[83] J. Xu, Y. Zhang, Z. Huang, C. Jia, S. Wang, *Energy Fuels* **2021**, *35*, 8617.
[84] S. W. Shaner, M. Islam, M. B. Kristoffersen, R. Azmi, S. Heissler, M. Ortiz-Catalan, J. G. Korvink, M. Asplund, *Biosens. Bioelectron. X* **2022**, *11*, 100143.
[85] J. Li, Y. Liu, L. Yuan, B. Zhang, E. S. Bishop, K. Wang, J. Tang, Y.-Q. Zheng, W. Xu, S. Niu, L. Beker, *Nature* **2022**, *606*, 94.
[86] E. Stavrinidou, P. Leleux, H. Rajaona, D. Khodagholy, J. Rivnay, M. Lindau, S. Sanaur, G. G. Malliaras, *Adv. Mater.* **2013**, *25*, 4488.
[87] H. Yuk, B. Lu, S. Lin, K. Qu, J. Xu, J. Luo, X. Zhao, *Nat. Commun.* **2020**, *11*, 1604.
[88] R. de Levie, *Electrochim. Acta* **1963**, *8*, 751.
[89] R. de Levie, *Electrochim. Acta* **1965**, *10*, 113.
[90] R. de Levie, *Electrochim. Acta* **1964**, *9*, 1231.
[91] J. J. Montero-Rodríguez, D. Schroeder, W. Krautschneider, R. Starbird, *Proceedings of the 6th IEEE Germany Student Conference,* Hamburg, Germany, Vol. *28*, **2015**.
[92] R. Hass, J. García-Cañadas, G. Garcia-Belmonte, *J. Electroanal. Chem.* **2005**, *577*, 99.
[93] J. Bobacka, A. Lewenstam, A. Ivaska, *J. Electroanal. Chem.* **2000**, *489*, 17.
[94] M. A. Vorotyntsev, J. P. Badiali, G. Inzelt, *J. Electroanal. Chem.* **1999**, *472*, 7.
[95] D. Loveday, P. Peterson, B. Rodgers, *JCT Coatingstech* **2005**, *2*, 22.
[96] J. Agrisuelas, C. Gabrielli, J. J. García-Jareño, H. Perrot, O. Sel, F. Vicente, *Electrochim. Acta* **2015**, *164*, 21.
[97] N. Yang, C. G. Zoski, *Langmuir* **2006**, *22*, 10338.
[98] J. L. Bredas, G. B. Street, *Acc. Chem. Res.* **1985**, *18*, 309.
[99] E. Stavrinidou, M. Sessolo, B. Winther-Jensen, S. Sanaur, G. G. Malliaras, *AIP Adv.* **2014**, *4*, 017127.